

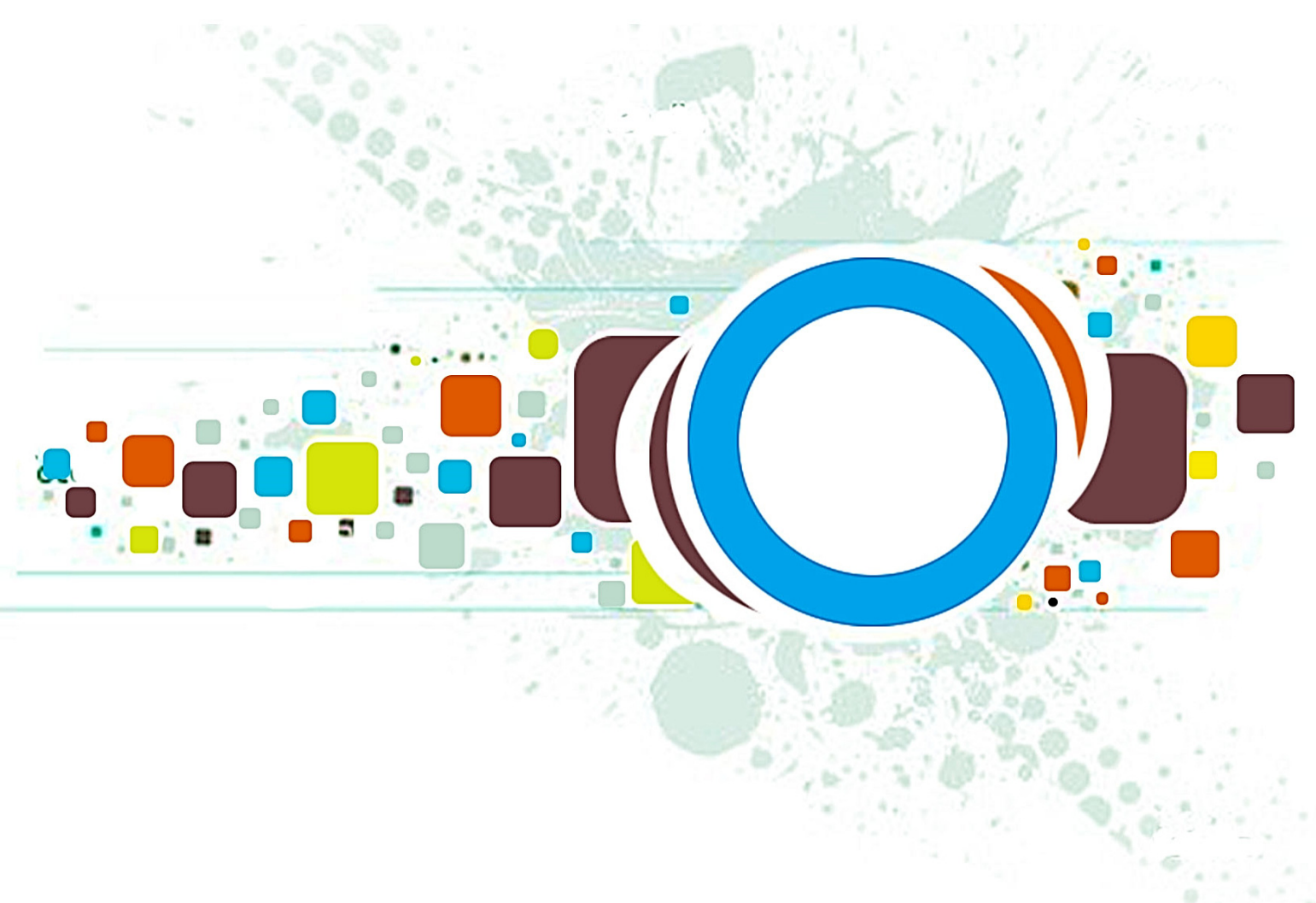
Volume 8 • Issue 2 • March 2014

Editor-in-Chief  
Professor Hu, Yu-Chen

INTERNATIONAL JOURNAL OF  
**IMAGE PROCESSING (IJIP)**

ISSN : 1985-2304

Publication Frequency: 6 Issues Per Year



CSC PUBLISHERS  
<http://www.cscjournals.org>

# **INTERNATIONAL JOURNAL OF IMAGE PROCESSING (IJIP)**

**VOLUME 8, ISSUE 2, 2014**

**EDITED BY  
DR. NABEEL TAHIR**

ISSN (Online): 1985-2304

International Journal of Image Processing (IJIP) is published both in traditional paper form and in Internet. This journal is published at the website <http://www.cscjournals.org>, maintained by Computer Science Journals (CSC Journals), Malaysia.

IJIP Journal is a part of CSC Publishers

Computer Science Journals

<http://www.cscjournals.org>

## **INTERNATIONAL JOURNAL OF IMAGE PROCESSING (IJIP)**

Book: Volume 8, Issue 2, March 2014

Publishing Date: 19-03-2014

ISSN (Online): 1985-2304

This work is subjected to copyright. All rights are reserved whether the whole or part of the material is concerned, specifically the rights of translation, reprinting, re-use of illustrations, recitation, broadcasting, reproduction on microfilms or in any other way, and storage in data banks. Duplication of this publication of parts thereof is permitted only under the provision of the copyright law 1965, in its current version, and permission of use must always be obtained from CSC Publishers.

IJIP Journal is a part of CSC Publishers

<http://www.cscjournals.org>

© IJIP Journal

Published in Malaysia

Typesetting: Camera-ready by author, data conversion by CSC Publishing Services – CSC Journals, Malaysia

**CSC Publishers, 2014**

## EDITORIAL PREFACE

The International Journal of Image Processing (IJIP) is an effective medium for interchange of high quality theoretical and applied research in the Image Processing domain from theoretical research to application development. This is the *Second* Issue of Volume *Eight* of IJIP. The Journal is published bi-monthly, with papers being peer reviewed to high international standards. IJIP emphasizes on efficient and effective image technologies, and provides a central for a deeper understanding in the discipline by encouraging the quantitative comparison and performance evaluation of the emerging components of image processing. IJIP comprehensively cover the system, processing and application aspects of image processing. Some of the important topics are architecture of imaging and vision systems, chemical and spectral sensitization, coding and transmission, generation and display, image processing: coding analysis and recognition, photopolymers, visual inspection etc.

The initial efforts helped to shape the editorial policy and to sharpen the focus of the journal. Started with Volume 8, 2014, IJIP appears with more focused issues. Besides normal publications, IJIP intends to organize special issues on more focused topics. Each special issue will have a designated editor (editors) – either member of the editorial board or another recognized specialist in the respective field.

IJIP gives an opportunity to scientists, researchers, engineers and vendors from different disciplines of image processing to share the ideas, identify problems, investigate relevant issues, share common interests, explore new approaches, and initiate possible collaborative research and system development. This journal is helpful for the researchers and R&D engineers, scientists all those persons who are involve in image processing in any shape.

Highly professional scholars give their efforts, valuable time, expertise and motivation to IJIP as Editorial board members. All submissions are evaluated by the International Editorial Board. The International Editorial Board ensures that significant developments in image processing from around the world are reflected in the IJIP publications.

IJIP editors understand that how much it is important for authors and researchers to have their work published with a minimum delay after submission of their papers. They also strongly believe that the direct communication between the editors and authors are important for the welfare, quality and wellbeing of the Journal and its readers. Therefore, all activities from paper submission to paper publication are controlled through electronic systems that include electronic submission, editorial panel and review system that ensures rapid decision with least delays in the publication processes.

To build its international reputation, we are disseminating the publication information through Google Books, Google Scholar, Directory of Open Access Journals (DOAJ), Open J Gate, ScientificCommons, Docstoc and many more. Our International Editors are working on establishing ISI listing and a good impact factor for IJIP. We would like to remind you that the success of our journal depends directly on the number of quality articles submitted for review. Accordingly, we would like to request your participation by submitting quality manuscripts for review and encouraging your colleagues to submit quality manuscripts for review. One of the great benefits we can provide to our prospective authors is the mentoring nature of our review process. IJIP provides authors with high quality, helpful reviews that are shaped to assist authors in improving their manuscripts.

### **Editorial Board Members**

International Journal of Image Processing (IJIP)

## **EDITORIAL BOARD**

**EDITOR-in-CHIEF (EiC)**

**Professor Hu, Yu-Chen**  
Providence University (Taiwan)

### **ASSOCIATE EDITORS (AEiCs)**

---

**Professor. Khan M. Iftekharruddin**  
University of Memphis  
United States of America

**Assistant Professor M. Emre Celebi**  
Louisiana State University in Shreveport  
United States of America

**Assistant Professor Yufang Tracy Bao**  
Fayetteville State University  
United States of America

**Professor. Ryszard S. Choras**  
University of Technology & Life Sciences  
Poland

**Professor Yen-Wei Chen**  
Ritsumeikan University  
Japan

**Associate Professor Tao Gao**  
Tianjin University  
China

**Dr Choi, Hyung Il**  
Soongsil University  
South Korea

### **EDITORIAL BOARD MEMBERS (EBMs)**

---

**Dr C. Saravanan**  
National Institute of Technology, Durgapur West Benga  
India

**Dr Ghassan Adnan Hamid Al-Kindi**  
Sohar University  
Oman

**Dr Cho Siu Yeung David**

Nanyang Technological University  
Singapore

**Dr. E. Sreenivasa Reddy**  
Vasireddy Venkatadri Institute of Technology  
India

**Dr Khalid Mohamed Hosny**  
Zagazig University  
Egypt

**Dr Chin-Feng Lee**  
Chaoyang University of Technology  
Taiwan

**Professor Santhosh.P.Mathew**  
Mahatma Gandhi University  
India

**Dr Hong (Vicky) Zhao**  
Univ. of Alberta  
Canada

**Professor Yongping Zhang**  
Ningbo University of Technology  
China

**Assistant Professor Humaira Nisar**  
University Tunku Abdul Rahman  
Malaysia

**Dr M.Munir Ahamed Rabbani**  
Qassim University  
India

**Dr Yanhui Guo**  
University of Michigan  
United States of America

**Associate Professor András Hajdu**  
University of Debrecen  
Hungary

**Assistant Professor Ahmed Ayoub**  
Shaqra University  
Egypt

**Dr Irwan Prasetya Gunawan**  
Bakrie University  
Indonesia

**Assistant Professor Concetto Spampinato**  
University of Catania  
Italy

**Associate Professor João M.F. Rodrigues**

University of the Algarve  
Portugal

**Dr Anthony Amankwah**

University of Witswatersrand  
South Africa

**Dr Chuan Qin**

University of Shanghai for Science and Technology  
China

**Associate Professor Vania Vieira Estrela**

Fluminense Federal University (Universidade Federal Fluminense-UFF)  
Brazil

**Dr Zayde Alcicek**

firat university  
Turkey

**Dr Irwan Prasetya Gunawan**

Bakrie University  
Indonesia

## TABLE OF CONTENTS

Volume 8, Issue 2, March 2014

### Pages

- |         |  |
|---------|--|
| 17 - 29 | Reeb Graph for Automatic 3D Cephalometry<br><i>Mestiri Makram, Hamrouni Kamel</i>  |
| 30 - 48 | Qualitative and Quantitative Evaluation of Two New Histogram Limiting Binarization Algorithms<br><i>Jan Brocher</i>  |
| 49 - 65 | Comparative Performance of Image Scrambling in Transform Domain using Sinusoidal Transforms<br><i>H. B. Kekre, Tanuja Sarode, Pallavi N Halarnkar, Debkanya Mazumder</i> |

# Reeb Graph for Automatic 3D Cephalometry

**Mestiri Makram**

*Enit/Electrical/Image Processing  
Enit  
Elnasr 2, 2037, Tunisia*

*mmestiri@gmail.com*

**Hamrouni Kamel**

*Enit/Electrical/Image Processing  
Enit  
Elnasr 2, 2037, Tunisia*

*Hamrouni.kamel@lsts.com*

---

## Abstract

The purpose of this study is to present a method of three-dimensional computed tomographic (3D-CT) cephalometrics and its use to study cranio/maxilla-facial malformations. We propose a system for automatic localization of cephalometric landmarks using reeb graphs. Volumetric images of a patient were reconstructed into 3D mesh. The proposed method is carried out in three steps: we begin by applying 3d mesh skull simplification, this mesh was reconstructed from a head volumetric medical image, and then we extract a reeb graph. Reeb graph mesh extraction represents a skeleton composed in a number of nodes and arcs. We are interested in the node position; we noted that some reeb nodes could be considered as cephalometric landmarks under specific conditions. The third step is to identify these nodes automatically by using elastic mesh registration using “thin plate” transformation and clustering. Preliminary results show a landmarks recognition rate of more than 90%, very close to the manually provided landmarks positions made by a medical staff.

**Keywords:** Reeb Graph, Cephalometry Landmarks, Thin Plate, LCP.

---

## 1. INTRODUCTION

Radiographic cephalometry has been one of the most important diagnostic tools in maxillofacial diseases, since its introduction in the early 1930. It deals with the morphological scientific study of the dimensions of all the structures present in a human head, usually through the use of standardized lateral head radiographs. Generations of doctors have relied on the interpretation of these images for their diagnosis and treatment planning as well as for the long-term follow-up of growth and treatment results. Also in the planning for surgical orthodontic corrections of jaw discrepancies, lateral/antero-posterior cephalograms have been valuable tools.

Parameters measurement is based on a set of agreed upon feature point's landmarks. The detection of the landmarks plays an essential role in diagnosis and treatment planning by doctors. Head-growing analyzing with anatomical landmarks was first proposed by Arc Thomson, in 1917 [1]. His approach was based on a deforming grid. Changes in the landmarks position resulted in deformations of the grid. His method was applied not only to quantify the effects of growth, but also to relate different individuals and even different species. A malocclusion is a misalignment of teeth or incorrect relation between the teeth of the two dental arches, Broadbent [2] and later Brodie [3] applied a method based in landmarks to quantify malocclusions and study their effects.

They used radio-graph image to define the Landmarks, head structure like bony or soft tissue, had to be identified. This approach was used for measurement specification at an individual of known age, sex and race to quantify head anatomy differences for diagnosis, such as the one shown in Figure 1.

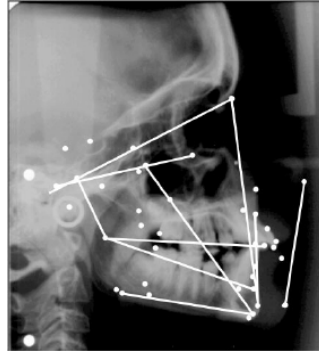


**FIGURE 1:** Manual Extraction of Cephalometry Landmarks in X-ray Image.

Downs [4] proposed in 1948 the first cephalometric analysis method. His approach was based on measurements of 10 angles from a lateral radiographs from a group of selected individuals; he calculates the average values and gives them a clinical significance. His approach was the basis for most methods used at present.

Ricketts [5] and Steiner [6] proposed traced lines between significant landmarks, so their length and angles can be measured and compared with standard values shown in Figure 2.

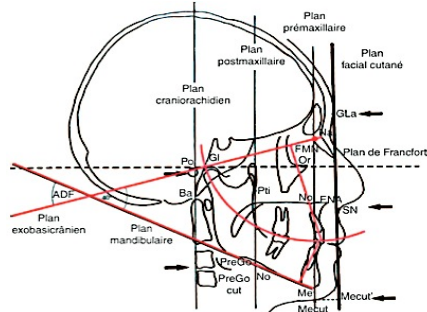


**FIGURE 2:** Line Traced Between Significant Landmarks [6].

Locating landmarks depends on medical expertise to locate the landmarks manually. This can take an experienced orthodontist up to 30 min. The process is time consuming, subject to human error and tedious.

An automated system would help to eliminate the above-mentioned problems and hence produce repeatable results.

## 2. RELATED WORKS

All the automatic cephalometric landmarks recognition methods use 2D image processing, the various methods used by researchers in this field found in the literature can be divided into three different approaches: knowledge-based feature detection, pattern matching and neural networks with fuzzy inference system.

Levy [7] proposed in 1986 the first automatic extraction of cephalometric landmarks. His method was based on knowledge based line extraction technique. He begins with applying median filter and histogram equalization to enhance the X-rays images, then he applies a Mero-Vassy operator [8] to extract relevant edges using knowledge-based line tracker. The landmarks are then located according to their geometric definition online crossing. This method requires good X-rays image (cannot be guaranteed in practice). Parthasaraty [9] proposed an enhancement of levy approach by introducing a multi resolution pyramidal analysis of X-rays images to reduce the processing time.

Yen [10], Contereras [11], Jackson [12], Cohen [13] and Davis and Forsyth [14] presented similar knowledge-based edge tracking methods. These methods depend highly on X-ray image quality and can be used only for landmarks located on an edge.

The second approach used mathematical or statistical models to narrow down the search area for each landmark, and then shape-matching techniques are used to locate the exact location of each landmark. Cardillo and Sid-Ahmed [15] proposed a method based on a combination of mathematical modeling methods, like affine transformation to remove the shifts, rotations and size differences to reduce the size of the search area. Then, they applied a shape recognition algorithm based on gray-scale mathematical morphology to locate the landmarks. The method locates 76% of the landmarks within 2 mm. Grauetal[16], adds a line detection module to select the most significant lines in Sid-Ahmed[15] approach. Then, he applies mathematical morphology transformations for shape recognition. The disadvantage of these methods is that it's very sensitive to noise present in X-rays images. Desvignes [17] proposed a statistical method based on estimation of landmarks locations using adaptive coordinate space where locations are registered. The method was tested on a set of 58 X-rays, of which 28 were used for training. They obtain 99.5% of the landmarks but with 4.5 mm mean error between the real position and the estimated position, far from the authorized range ( $\pm 2$  mm). Hutton [18] used active shape models for cephalometric landmarking. They established a template of possible deformations from a training set of hand-annotated image. The result was 35% of 16 landmarks within an acceptable range of  $\pm 2$  mm. Implementation could be used as a first estimation location of the landmarks.

The third category of researchers used neural networks and fuzzy inference systems to locate the landmarks. Uchino [19] proposed a fuzzy learning machine that could learn the relation between the gray levels of the image and the location of the landmarks. They begin by dividing the image into nine blocks, each one is an input to the fuzzy learning machine. The weights were adjusted by learning the coordinates of the landmark. The block containing the landmark was divided in nine separate blocks until landmark location is obtained. This method produced an average error of 2.3 mm. this method depends highly on scale, rotation and shift of X-rays images. Innes [20] highlights regions containing craniofacial features using Pulse Coupled Neural Networks (PCNN) from X-rays images. They get 36.7% rate for the region containing sella landmark, 88.1% for the region containing the chin landmark, and 93.6% for the region containing the nose landmark. The most disadvantage of PCNN's method is that they require a considerable manual contribution to set the required parameters.

In this paper, we are interested in the extension of 2D X-rays to 3D image cephalometry analysis. Some work has been carried out to study the potential advantages of 3D imaging methods, such as computed tomography for cephalometric analysis. Kragsskov [21] made a comparative result, using human dry skulls. Ferrario [22] studied 3D facial morphometry using infrared cameras, but only as a supplement for classic cephalometry.

We propose a novel method based on the use of reeb graph for Automatic localization of craniofacial landmarks. The task is a difficult one due to the complexity and variability of cephalometry landmarks.

### 3. PROPOSED METHOD

As seen in previous works, many researchers have attempted automatic cephalometric landmarks detections. However, a major drawback of the existing techniques is that they use a 2D representation of a 3D structure. In this paper we are interested in a 3D cephalometric landmarks. The development of spiral CT and cone beam CT has revolutionized the medical image techniques, the former providing outstanding resolution and the latter, with its low cost, allowing unique accessibility, as a result 3-D imaging has become an essential tool in planning and managing the treatment of facial deformity.

#### 3.1 3D Mesh Database

The image data-base is composed of Dicom images stored in a series of 2D grey level images from a Spiral CT scan (with 512 x 512 matrixes, 110 kV, and 80 mAs) performed at 1 mm slice thickness. The extraction of hard and soft head tissue (bones and skin) is done by using a threshold and region growing technique. Each bones and skin parts are separately constructed using marching cube algorithm as shown in Figure 3.

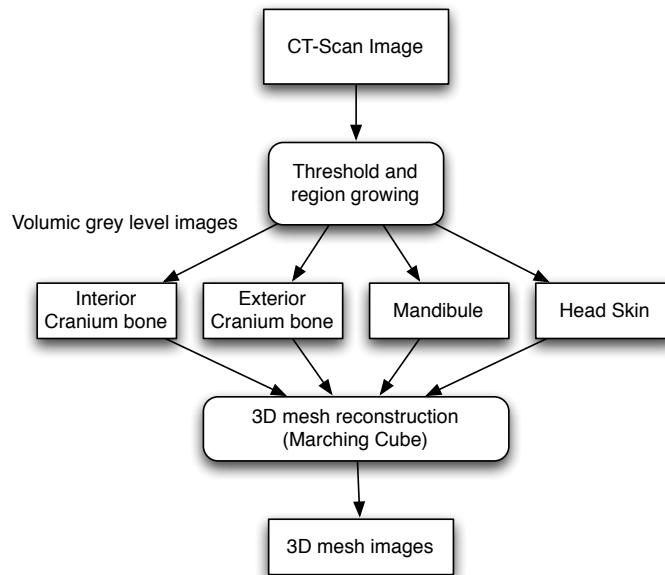


**FIGURE 3:** 3D Mesh Extraction of Hard and Soft Tissues.

The results of this extraction method are 3 meshes: interior/exterior skull bones, and mandibular bone Figure-4.

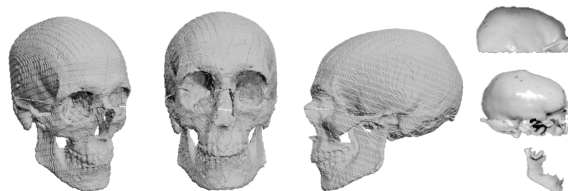


**FIGURE 4:** 3D Mesh Extraction from Volumetric CT-Scan .

#### 3.2 3D Cephalometric Landmarks

After getting the mesh database, 3D cephalometric landmarks must be localized in hard tissue. In the literature we found 20 hard landmarks, some of them are presented in table-1.

No	Abbreviation	Hard Tissue
1	N	Nasion is the midpoint of the frontonasal suture
2	S	Sella is the centre of the hypophyseal fossa (sella turcica).
3	Po	Porion is the most superior point of each external acoustic meatus.
4	Or	Orbitale is the most inferior point of each infra- orbital rim.
5	ANS	Anterior Nasal Spine is the most anterior midpoint of the anterior nasal spine of the maxilla.
6	PNS	Posterior Nasal Spine is the most posterior midpoint of the posterior nasal spine of the palatine bone.
7	PMP	Posterior Maxillary Point is the point of maximum concavity of the posterior border of the palatine bone in the horizontal plane at both sides.
8	UI	Upper Incisor is the most mesial point of the tip of the crown of each upper central incisor.
9	LI	Lower Incisor is the most mesial point of the tip of the crown of each lower central incisor.
10	UMcusp	Upper Molar cusp is the most inferior point of the mesial cusp of the crown of each first upper molar in the profile plane.

**TABLE 1:** 10 of the 20 Cephalometric Landmarks Proposed by Swennen [23].

Figure 5 shows some sample of CT-scan images with located landmarks [23].

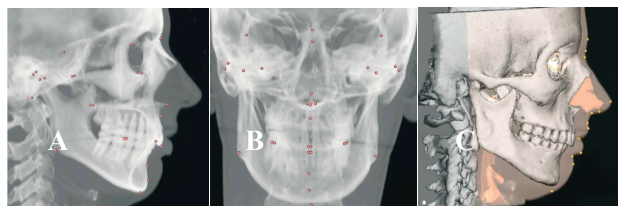


**FIGURE 5:** A: Right hard cephalometric landmarks, B: Facial hard cephalometric landmarks, C: Soft cephalometric landmarks.

### 3.3 Automatic Localization of Craniofacial Landmarks

Figure 6 presented the bloc diagram of the proposed method for automatic localization of 3D cephalometric landmarks.

After transforming the volumetric medical images to a 3D surface mesh, we need to make a reference shape model containing all cephalometric landmarks information's. This is made with what is called "cephalometric head atlas".

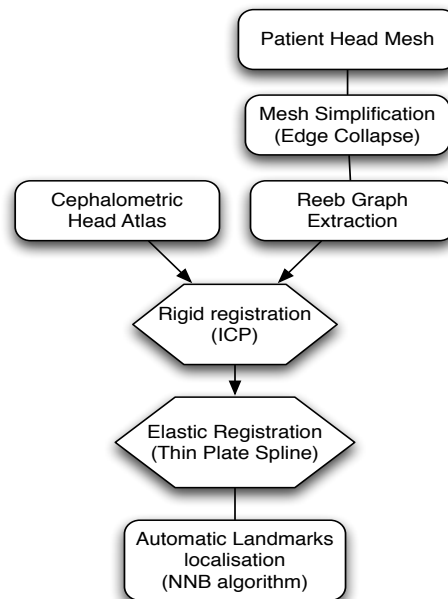


**FIGURE 6:** Automatic localization of 3D cephalometric landmarks using reeb graphs.

To automatically identify 3D landmarks, we need to have prior knowledge information's. We create a cephalometric head atlas based on medical stuff help. This atlas is composed of skull and skin meshes with 3D cephalometric landmarks as shown in Figure 7.

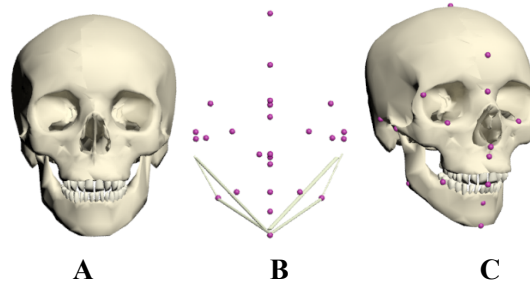


**FIGURE 7:** Cephalometric atlas of skull. A: initial clean skull mesh, B: Cephalometric landmarks and C: Manual localization of cephalometric landmarks.

In our method we choose to automatically localize cephalometric landmarks using reeb graph. Below we will expose the reeb graph extraction.

The Reeb graph is a chart of connectivity on a surface between its critical points. The main advantage of the reeb graph is that it makes it possible to represent 3D anatomy in a simple topology way. It is composed of nodes and arcs; each whole of level associates a node. The graph of Reeb is obtained starting from the computation of a  $\mu$  function introduced by the theory of Morse [24] defined on the closed surface of an object in its critical points [25].

We define  $\mu: S \rightarrow R$  defined on surface  $S$  of a 3D object. The Reeb graph is a space quotient of the graph of  $\mu$  in  $S$ , defined by the relation of following equivalence between  $X \in S$  and  $Y \in S$ :

$$X \sim Y \Leftrightarrow \begin{cases} \cdot \mu(X) = \mu(Y) \\ \cdot X \text{ et } Y \text{ are in the same Related component of } \mu^{-1}(\mu(X)), \text{ and the image } \mu(Y) \text{ is } S. \end{cases} \quad (1)$$

The aspect of the graph is entirely related to the choice of the  $\mu$  function, which determine the properties of stability and invariance of the resulting graphs. Several functions of application were proposed in the state of the art for the construction of Reeb graphs [26]. One example is the function ( $\mu(v(x,y,z)) = z / v \in S$ ), adapted well for the models whose points are mainly distributed in the Z-axis direction.

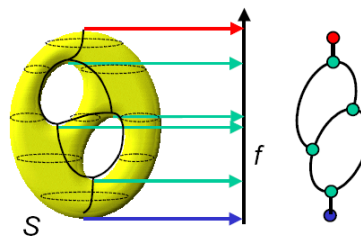


**FIGURE 8:** Reeb Graph with a z Projection  $\mu$  Function.

The function suggested in [27] as «outdistances geodesic extrema of curve » is based on growth of areas starting from local Gaussian curves on tops (germs). The results depend on the position of the germs and require no disturbed data; it's a precise calculation of the local curves. Hilaga [27] defines a function by computing the distance from a point of the surface to the center of mass G of the object:

$$(\mu(v) = d(G, v) / v \in S \text{ et } d : \text{Euclidian distance}) \quad (2)$$

The function defined by Thierny[28] at the characteristic points and the geodesic distances is defined by the following equation:

$$\mu(v) = 1 - \delta(v, v_p) \quad (3)$$

$$\text{With } \delta(v, v_p) = \min_{v_{fi} \in F} \delta(v, v_{fi})$$

Where  $\delta$  is the function of the geodesic distances and  $v_p$  are characteristic points. The function suggested in [29] is the integral of the geodesic distances  $g(v, p)$  of  $v$  to the other point's  $p$  of the surface (4).

$$\mu(v) = \int_{p \in S} g(v, p) dS. \quad (4)$$

In our approach we choose this  $\mu$  function and tested it with different mesh simplification. Figure-9 shows an example of reeb graph extraction.

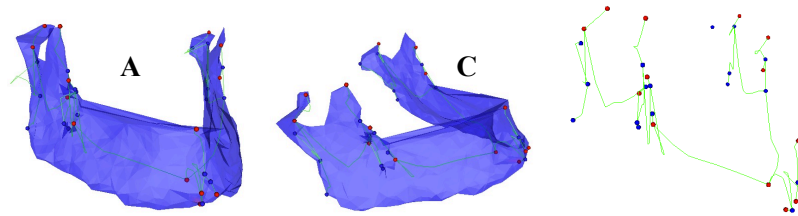


FIGURE 9: A: Mandibule Patient Mesh, B: Reeb Graph Extraction.

Surface mesh simplification is the process of reducing the faces number used in the mesh surface, while keeping preserved as much as possible the overall shape, volume and boundaries. Cignoni [29] proposed a comparison of mesh simplification algorithms, and divided these methods into 7 approaches: coplanar facets merging, controlled vertex/edge/face decimation, retiling, energy function optimization, vertex clustering, wavelet-based approaches, and simplification via intermediate hierarchical representation.

We test many simplification methods with reeb graph transformation, and we choose to use the edge collapse method. These techniques reduce a model's complexity by repeated use of the simple edge collapse operation. Researchers have proposed various methods of determining the "minimal cost edge" to collapse at each step (figure-10).

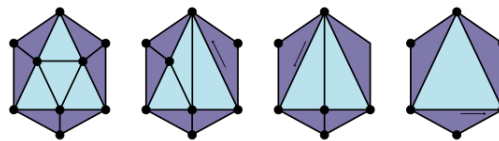
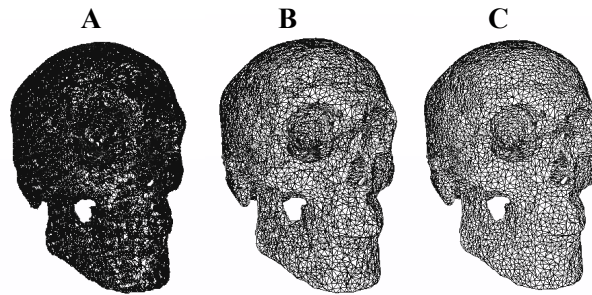


FIGURE 10: Edge Collapse Algorithm [30].

We try to define the effect of the edge collapse simplification process on the reeb graph extraction. The result is shown in figure-11



**FIGURE 11:** Patient Skull Simplification. A: 332.932 vertices and 662.564 faces, B: 20.047 vertices and 38.958 faces and C: 3.887 vertices and 7320 faces.

We notice that, after mesh simplification, the number of nodes in the reeb graph decreased and they became closed to cephalometric landmarks. And, of course, the computation time is reduced Figure-12.

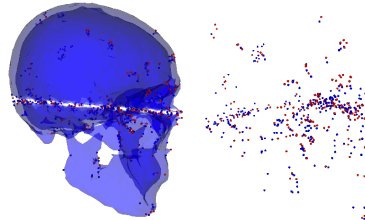


**FIGURE 12:** Decrease of reeb graph nodes and reconciliation with cephalometric landmarks.

Mesh registration is a technique used to find a transformation for mapping a source mesh known as a reference mesh and a target mesh. This technique associated to a head cephalometric atlas should help us to get closer to cephalometric landmarks. Every elastic registration process should begin with a rigid one. In this study, we targeted the rigid registration between two different meshes using the ICP algorithm (Iterative Closest Point).

The principle of ICP is to iterate between a step of mapping data and another step of optimization of rigid transformation until convergence. The transformation used for registration is composed of a 3D rotation and translation. At each iteration, the Algorithm provides a list of matched points and an estimate of the transformation. The algorithm converges when the error in distance between matched points is less than a given threshold. The ICP algorithm is presented in the following [30] where  $N_p$  is the number of points CP1 and CP2 and  $k$  is the index of current iteration. Figure-13 shows a example of rigid registration between mesh patient and cephalometric mesh atlas.

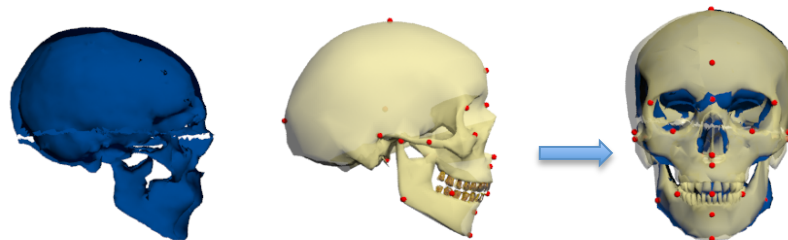


**FIGURE 13:** Rigid registration between patient and the cephalometric atlas

Mesh elastic registration is a mesh deformation process; one of the transformations that are able to represent elastic deformations is the thin-plate spline (TPS). Thin plate splines were introduced by Bookstein[31] for geometric design. In 2D images, the TPS model describes the transformed coordinates (xT,yT) both independently as a function(7) of the original coordinates (x, y):  
 $(xT,yT)=(fx(x,y),fy(x,y))$  (7)

The algorithm begins with a given displacements of a number of landmark points, the TPS model interpolates those points, while maintaining maximal smoothness. For each landmark point (x,y), the displacement is represented by an additional z-coordinate, and, for each point, the thin plate is fixed at position (x, y, z). The strain energy is calculated by integrating the second derivative over the entire surface that can be minimized by solving a set of linear equations.

$$\iint_{\pi^2} \left( \left( \frac{\partial^2 z}{\partial x^2} \right)^2 + 2 \left( \frac{\partial^2 z}{\partial x \partial y} \right)^2 + \left( \frac{\partial^2 z}{\partial y^2} \right)^2 \right) dx dy$$
 (8)

The TPS model for one of the transformed coordinates is given by parameter vectors a and D (9):

$$F(xT,yT)= a1+a2x+a3y+...+ \sum_{i=1}^n D_i F(L_i - (x, y))$$
 (9)

Where  $F(r)= r2\log(r)$  is the basis function,  $a = [a1 a2 a3 a4]T$  defines the affine part of the transformation, D gives an additional non-linear deformation, and the  $L_i$  are the landmarks that the TPS interpolates figure-4.

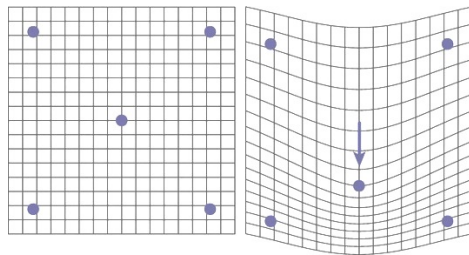


**FIGURE 14:** A template configuration (left) and a target configuration (right) of five landmarks each.

The deformation right grid illustrates the thin-plate spline function between these configurations as applied to the left regular grid.

The method interpolates some of the points using smoother transformation controlled by a parameter  $\mu$ , which weights the optimization of landmark distance and smoothness. For  $\mu = 0$ , there is full interpolation, while for very large  $\mu$ , there is only an affine transformation. In our methods the landmarks used in the TPS algorithm are the reeb graph nodes as shown in figure-15.

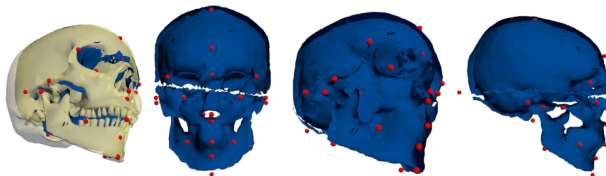


**FIGURE 15:** Elastic Registration using Thin Plate.

As result of the elastic registration, the patient reeb graph nodes become closer to the atlas cephalometric head landmarks. Since, some reeb graph nodes are not cephalometric landmarks, we have to select the real ones.

**Automatic localization of cephalometry landmarks**

This step starts with the creation of possible landmark localization in cephalometric atlas. Then, it identifies the reeb graph nodes that exist in the mesh patient. For each node, it searches the closest landmarks in the cephalometric atlas through the calculation of Euclidean distance between an acceptable range of  $\pm 2$  mm. Finally, as a result all patient reeb graph nodes are associated to a nearest cephalometric landmarks[32].

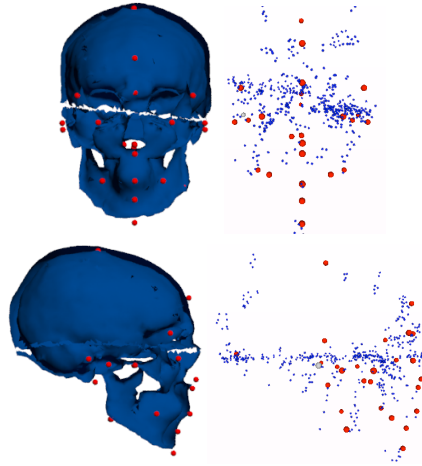


**FIGURE 16:** Localization of Cephalometric Landmarks in Patient Skull.

**4. TEST AND RESULTS**

To validate our approach we asked a doctor to conduct manually a cephalometric analysis on the mesh patient. We then calculate the error between its points and cephalometric landmarks automatically localized by our method. The result is showed in the following table:

No	Abbreviation	Error in mm	Recognized
1	N	0.5	Yes
2	S	2.6	No
3	Po	1.3	Yes
4	Or	0.4	Yes
5	ANS	0.7	Yes
6	PNS	2.8	No
7	PMP	2	Yes
8	UI	1.3	Yes
9	LI	1.7	Yes
10	UMcusp	1.8	Yes
11	LMcusp	0.9	Yes
12	Men	0.8	Yes
13	Go	1.5	Yes
14	Fz	1.7	Yes
15	Zy	0.3	Yes
16	A	0.4	Yes
17	B	0.5	Yes
18	Pog	0.8	Yes
19	Ba	0.6	Yes
20	Co	1.4	Yes

**TABLE 2:** Result of cephalometric landmarks detection

Our method localized 18 landmarks on 20. This mean a percentage of 90% landmarks in patient mesh was recognized.

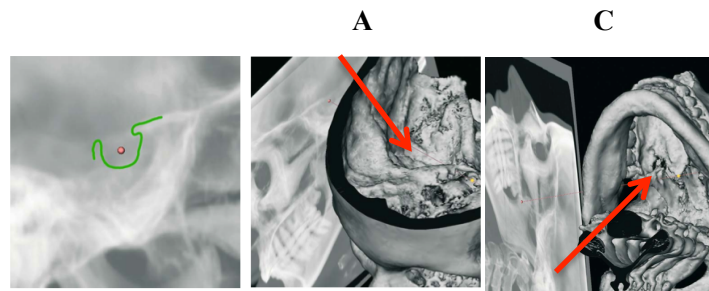


**FIGURE 17:** Localization of A- Sella and B- PNS Landmarks.

The Sella landmark (S) is very difficult to be localized. It is not localized in the surface mesh, and the doctors need to insert it taking into account the interior skull surface. The Posterior Nasal Spine Landmark (PNS) is defined on the exo-cranial skull base view of the 3-D hard tissue surface representation. This landmark depends highly on the accuracy of the mesh reconstruction.

## 5. CONCLUSION

In this paper, we have proposed a novel method for automatic 3D localization of cephalometric landmarks. Our approach is based on reeb graph nodes. In particular, we have presented results for localized 90% of cephalometric landmarks in CT-Scan medical images. We initiated a new approach for automatic three-dimensional cephalometric analysis. The proposed method needs to be validated on a larger database.

## 6. REFERENCES

- [1] A.Thomson « On growth and form ». Cambridge, UK: Cambridge Univ. Press, 1992.
- [2] Broadbent HB. « A new X-ray technique and its application to orthodontia ». Angle Orthod 1931;
- [3] Brodie AG. « On the growth pattern of the human head from the third month to the eighth year of life ». Am J Anat 1941; 68:209–62.
- [4] Downs WB. « Variations in facial relationships: their significance in treatment and prognosis ».Am J Orthod 1948; 34:812–40.
- [5] Ricketts RM. « Cephalometric Analysis and Synthesis ». Angle Orthod, 1961; 31:141–56.
- [6] Steiner C. « Cephalometrics in clinical practice ». Angle Orthod 1959; 29:8–29.
- [7] A. Levy-Mandel, A. Venetsanopoulos, J. Tsotsos, « Knowledge-based landmarking of cephalograms », Comput. Biomed. Res. 19 (3) (1986) 282–309.
- [8] L. Mero, Z. Vassy, « A simplified and fast version of the Hueckel operator for finding optimal edges in pictures », Proceedings of the Fourth International Joint Conference on Artificial Intelligence, Tbilissi, Georgia, USSR, September 1975, pp. 650–655.
- [9] S. Parthasaraty, S. Nugent, P.G. Gregson, D.F. Fay, « Automatic landmarking of cephalograms », Comput. Biomed. Res. 22 (1989) 248–269.

- [10] C.K. Yan, A. Venetsanopoulos, E. Filleray, « An expert system for landmarking of cephalograms », Proceedings of the Sixth International Workshop on Expert Systems and Applications, 1986, pp. 337–356.
- [11] J.L. Contereras-Vidal, J. Garza-Garza, « Knowledge-based system for image processing and interpolation of cephalograms », Proceedings of the Canadian Conference on Electrical and Computer Engineering, 1990, pp. 75.11–75.14.
- [12] P.H. Jackson, G.C. Dickson, D.J. Birnie, Digital « image processing for cephalometric radiographic: a preliminary report », Br. J. Orthod. 12 (1985) 122
- [13] A.M. Cohen, A.D. Linney, « A low cost system for computer-based cephalometric analysis », Br. J. Orthod. 13 (1986) 105–108.
- [14] Forsyth D. D.Davis, « Knowledge-based cephalometric analysis: a comparison with clinicians using interactive computer methods», Comput. Biomed. Res. 27 (1994) 10–28.
- [15] M. Sid-Ahmed, J. Cardillo, « An image processing system for the automatic extraction of craniofacial landmarks », IEEE Trans. Med. Imaging 13 (2) (1994) 275–289.
- [16] V. Grautel, M.C. Juan, C. Monserrat, C. Knoll, « Automatic localization of cephalometric landmarks », J. Biomed. Inf. 34 (2001) 146–156.
- [17] M. Desvignes, B. Romaniuk, R. Demoment, M. Revenu, M.J. Deshayes, « Computer assisted landmarking of cephalometric radiographs », Proceedings of the Fourth IEEE Southwest Symposium on Image Analysis and Interpretation, 2000, pp. 296–300.
- [18] T.J. Hutton, S. Cunningham, P. Hammond, « An evaluation of active shape models for the automatic identification of cephalometric landmarks », Eur. J. Orthodont. 22 (5) (2000) 499–508.
- [19] E. Uchino, T. Yamakawa, « High speed fuzzy learning machine with guarantee of global minimum and its application to chaotic system identification and medical image processing », Proceedings of the Seventh International Conference on Tools with Artificial Intelligence, 1995, pp. 242–249.
- [20] A. Innes, V. Ciesielski, J. Mamutil, S. John, « Landmark detection for cephalometric radiology images using pulse coupled neural networks », International Conference in Computing in Communications, June 2002, pp. 391–396.
- [21] Kragstov J, Bosch C, Gyldensted « Comparison of the reliability of craniofacial anatomic landmarks based on cephalometric radiographs and 3-dimensional CT scans », Cleft Palate Crani- ofac J 1997; 34:111–6.
- [22] Ferrario VF, Sforza C, Poggio CE, « Facial 3-dimensional morphometry ». Am J Orthod Dentofac Orthop 1996; 109:86–93.
- [23] Gwen R. J. Swennen, Filip Schutyser, Jarg-Erich Hausamen « Three-dimensional cephalometry: a color atlas and manual » Amazon Book.
- [24] Milnor (j.w), « Morse theory », Princeton University Press, Princeton, NJ, (1963)
- [25] Reeb, G. « Sur les points singuliers d'une forme complètement intégrable ou d'une fonction numérique ». Livre stringer (1946).

- [26] Tony Tong Thèse « Indexation 3D de bases de données d'objets par graphes de Reeb améliorés » (2005)
- [27] Hilaga, Shigawa, « Topology Matching for fully automatic Similarity Estimation of 3D Shape », ACM SIGGRAPH, Los Angeles, CA, USA (2001).
- [28] J. Tierny, J. Vandeborne et M. Daouadi, « Graphe de Reeb de haut niveau de maillages polygonaux ». Journées de l'association Francophone d'informatique graphique, bordeaux (2006).
- [29] P. Cignoni, C. Montani, R. Scopigno : « A comparison of mesh simplification algorithms », Int. Symp. on 3D Data Processing, Visualization, and Transmission.
- [30] Besl P.J., McKay N.D., "A Method for Registration of 3D Shapes", IEEE Trans. On Pattern Analysis and Machine Intelligence (TPAMI), Vol.14(2), pp. 239-255,1992.
- [31] F. L. Bookstein, "Principal Warps: Thin-Plate Splines and the Decomposition of Deformations" IEEE Transaction on pattern analysis and machine intelligence. Vol 11, No 6, June 1989.
- [32] Makram Mestiri, Sami Bourouis and Kamel Hamrouni, "Automatic Mesh Segmentation using atlas projection and thin plate spline: Application for a Segmentation of Skull Ossicles", VISAPP 2011.

# Qualitative and Quantitative Evaluation of Two New Histogram Limiting Binarization Algorithms

**Jan Brocher**  
BioVoxel  
67112, Mutterstadt  
Germany

*jan.brocher@biovoxxel.de*

---

## Abstract

Image segmentation and thus feature extraction by binarization is a crucial aspect during image processing. The "most" critical criteria to improve further analysis on binary images is a least-biased comparison of different algorithms to identify the one performing best. Therefore, fast and easy-to-use evaluation methods are needed to compare different automatic intensity segmentation algorithms among each other. This is a difficult task due to variable image contents, different histogram shapes as well as specific user requirements regarding the extracted image features. Here, a new color-coding-based method is presented which facilitates semi-automatic qualitative as well as quantitative assessment of binarization methods relative to an intensity reference point. The proposed method represents a quick and reliable, quantitative measure for relative binarization quality assessment for individual images. Moreover, two new binarization algorithms based on statistical histogram values and initial histogram limitation are presented. This mode-limited mean (MoLiM) as well as the differential-limited mean (DiLiM) algorithms were implemented in ImageJ and compared to 22 existing global as well as local automatic binarization algorithms using the evaluation method described here. Results suggested that MoLiM quantitatively outperformed 11 and DiLiM 8 of the existing algorithms.

**Keywords:** Automatic Segmentation, Intensity Thresholds, Binarization Quality Assessment, Quantitative Segmentation Evaluation, ImageJ.

---

## 1. INTRODUCTION

Simple image segmentation by binarization methods have a long tradition and are broadly used in image processing. Generally, the binarization process is achieved by applying an intensity threshold dividing the image in two distinct regions, foreground and background. All objects of interest should thus be assigned to the foreground and the remaining parts of the image to the background. The aim of such methods in most cases is to extract features to be able to quantify object numbers, measure object sizes (e.g. area, length, area fractions, volumes surfaces), extracting text from documents or mask original images to specific regions retrieved from a binarized image. To achieve a high quality binarization with a reliable and good separation of foreground from background pixels depends first of all on the overall image quality. This is influenced by the lighting properties, objective quality, final resolution of the digital image, signal intensity, contrast and dynamic range as well as the objects' properties such as distance to neighboring objects, differences in intra-object intensities or the object-background intensity distribution. For most applications image pre-processing needs to be included to improve binarization. This might be done by using image filters to homogenize certain intensities while preserving object boundaries (e.g. applying a median convolution filter) or by background subtraction algorithms to eliminate unspecific signals. The latter is frequently necessary in fluorescent microscopic images from biological samples. Due to the availability of a plethora of processing methods the user always needs to be aware not to alter the primary image data too much to still preserve the objects properties before binarization to end up with a binary image which represents the objects of interest best. Manual segmentation in most image analysis software can be done by choosing a threshold value lying within the dynamic range of the image.

This theoretically leads to 255 different options in an 8-bit image and already 65536 possibilities in a 16-bit image. Thus, finding a reliable manual intensity threshold might be a tedious and user-biased procedure with the need to process each image individually. To be able to compare images of one series/experiment binarized by a manual threshold all images of that series would theoretically need to be segmented using the same upper and lower threshold values to prevent further increase in bias during image comparison. Those fixed thresholds will seldom lead to a satisfying overall outcome. The dependence on the image content and signal intensity rectifies the use of thresholds which take the pixel intensity distribution into account by basing the threshold choice on the images' histogram and its properties.

Therefore, many automatic thresholding methods of digital images have been proposed in the last decades [1], [2]. Automatic thresholds can be basically divided in global and local algorithms. Global algorithms normally use the complete image information for threshold determination and are applied to the complete image equally. Local algorithms, in contrast, determine various thresholds from different partitions of the image and/or contextual relations between those and allow varying threshold application in different image partitions.

The basic advantage of automatic thresholds is that they account for image variations and make a batch processing of many images easy without user bias.

Besides its long history and broad application, the topic of developing better new binarization algorithms as well as their qualitative and quantitative evaluation and comparison remains an active field of research and is extremely important to improve image analysis further.

Nevertheless, quality assessment of different binarization algorithms is not a simple task since certain evaluation criteria need to be specified in advance to allow quantitative evaluation of threshold performance. Thus, there is no real objective procedure to conduct such a comparison [3] since it furthermore depends on the nature of the scene or sample shown in the image and the needs of the user or the further analyses. There is also no perfect ground truth segmentation to which other methods could be compared [4].

Attempts of quality evaluation, mostly on grayscale images, have been made by using shape measures and region uniformity [1] or other criteria [5] as well as global image contrast and classification error calculations [6] or machine learning [7], [8]. The latter method for example is also based on the user input during the training session using example images and then performs an unsupervised evaluation based on the input. Other methods for completely unsupervised evaluation have a varying performance depending on the images and their content [7] and often need the previously created binary images.

The method presented here does not allow a completely unsupervised evaluation due to the necessity of a user-selected reference point based on pixel intensity. Besides a certain bias, this enables an individual quality assessment dependent on the image content as well as the user's needs for further analysis. The implementation in the Java based software ImageJ (and Fiji) allows a straight forward application to the original grayscale image. Several available binarization algorithms are applied at once to the image with the consecutive qualitative and quantitative evaluation and comparison.

The theory and algorithm of the qualitative and quantitative binarization evaluation method described here can be individually applied to all available automatic thresholding algorithms without any limitation to specific software, image contents or binarization performance.

## 2. MATERIAL AND METHODS

### 2.1 Qualitative and Quantitative Binarization Evaluation

The nature of any qualitative and quantitative evaluation procedure is to be able to separate true positive image areas from misclassified pixels. In the proposed method this separation is achieved by reference image pre-processing and color coding (2.1.1), definition of a relative quality reference intensity (2.1.2), color coding of the images to be evaluated and a consecutive (2.1.3) quantification of the pixel numbers in the individual image compartments classified as true positive, over-estimated (false positive), under-estimated (false negative) and background (true negative) (2.1.4).

#### 2.1.1 Reference Image Pre-processing and Color-coding

The color coding is done by first applying a green look-up-table (LUT) to a copy of the original image (figure 1A) such that all shades of gray are transferred to different intensities of green (intensity 0 = black). Furthermore, the image is slightly contrast enhanced by using linear histogram normalization with an over-saturation of 1% of the total pixel number (figure 1C). The slight over-saturation enables a better qualitative visual evaluation, especially for images with a very low over-all intensity. An over-saturation, inverse proportional to the average intensity of the image was also considered for those adjustments but did not lead to good visualization in images with a low over-all mean intensity.

For color coding two 24-bit RGB images of the same size as the original image are created. One is filled with pure red pixels (every pixel (R/G/B) = 255/0/0), the other is equally filled with pure blue pixels (every pixel (R/G/B) = 0/0/255). Thereafter, the pre-processed copy of the original image is combined with those two color images separately by an addition of the colors (figure 1D and E). These images simulate the color coding range of the original image with the following partitions:

True positive signals are depicted in yellow and bright orange while over-estimated (false positive) areas/objects are displayed in red and dark orange (figure 1B left and D). Under-estimated (false negative) areas/objects are coded in cyan and bright blue and background (true negative) is shown in dark blue (figure 1B right and E).

#### 2.1.2 Definition of the Relative Quality Reference Intensity

As a relative reference intensity in the given example in figure 1 the darkest intensity which is meant to still belong to the bright objects (and thus needs to be recognized as such) has to be carefully chosen by the user in the saturated copy of the original image (see 2.1.1). The color-coded images are then transferred into HSB color space and the hue channel serves for further processing.

To put the users' pixel selection in perspective and avoid over-sensitivity a 3x3 pixel area around the selected pixel is evaluated in the hue channels of the two reference images (schematically depicted in figure 1B). The mean value of these 9 pixels is taken as reference limit (figure 1B, black line between 'positive' and 'over' or 'under' and 'background', respectively). See also table 1 for the assessment of different reference values. Using the basic RGB-to-HSB conversion in ImageJ, an 8-bit image is used to represent the different hue channel values with obvious accuracy limitations in comparison to calculated floating point pixel values. Furthermore, 6 color values are combined in 1 hue value to completely represent the full individual color channel range. This mapped the 255 different shades from yellow to red to the hue channel intensity values 0-42 and cyan to blue to the hue channel intensity values 127-170, respectively.

The quality cut-off values retrieved from the two color-coded reference images according to the users' original reference point selection (indicated by the two-headed arrow in figure 1B to refer to its flexibility) serve as cut-off values to divide the evaluation partitions as shown in figure 1B.

A higher precision by calculating the individual hue channel floating point pixel values and using them as bases for the quantification was also evaluated but did not markedly improve the over-all evaluation performance (data not shown). In contrast, the time performance dropped massively which was further influenced by an increasing image size.

### 2.1.3 Color-coding of the Tested Image for Qualitative Evaluation

After performing the individual automatic thresholding methods the resulting binary images are color coded such that a red color (R/G/B = 255/0/0) is assigned to the foreground objects (figure 1F, G and H depicted in white) and a blue color (R/G/B = 0/0/255) is assigned to the background (figure 1F, G and H depicted in black). According to 2.1.1 the pre-processed copy of the original image is combined with those binary images resulting in the final color-coded images for qualitative visual evaluation (figure 1I, J and K). Those serve as a visual control for the final quantitative assessment.

### 2.1.4 Quantitative Assessment of Binarization Algorithms

According to the cut-off reference the pixel hue values ( $H_{u,v}$ ) at position  $I_{u,v}$  in the image are assigned to one of the four possible partitions:

$$(Eq. 1) \quad I_{u,v} = \begin{cases} \text{over-estimated (false positive)} & \text{if } 0 < H_{u,v} < \text{cut-off}_1 \\ \text{objects of interest (true positive)} & \text{if } \text{cut-off}_1 \leq H_{u,v} \leq 42 \\ \text{under-estimated (false negative)} & \text{if } 127 \leq H_{u,v} < \text{cut-off}_2 \\ \text{background (true negative)} & \text{if } \text{cut-off}_2 \leq H_{u,v} \leq 170 \end{cases}$$

with  $\text{cut-off}_1$  = value between 0 and 42 (range from red to yellow) and  $\text{cut-off}_2$  = value between 127 and 170 (range from cyan to blue)

The individual number of pixels assigned to the four partitions are used to calculate the percentage they cover in the complete image.

As a final quality parameter a measure was chosen equal to the one used by Shufelt [9]. This is:

$$(Eq.2) \quad \text{relative quality} = 100\% * \text{true positive} / (\text{true positive} + \text{false positive} + \text{false negative})$$

The relative quality can be used to figure out the binarization method(s) which perform(s) best in respect to the reference point selection in comparison to other thresholds.

## 2.2 Mode-Limited Mean (MoLiM) and Differential-Limited Mean (DiLiM) Algorithms

The new binarization algorithms proposed within this manuscript first assumes some premises on the histogram of the image to be binarized.

(1) For the MoLiM algorithm the histogram needs to have a mode value (the intensity value which occurs most frequently in the image). For the second modified version of the algorithm (DiLiM) a median or intermediate mean intensity value (mean\* see Eq. 3) might be calculated and used instead of the mode. The existence of a mode or a median value is true for all real images even in the artificial case of an image that contains the same intensity value in all pixels.

(2) It is made the assumption that the objects of interest cover the smaller part of the image (<50% of the total pixel number) while the background takes on >50% of all pixels. In the case of bright objects on a dark background this leads to a mode value smaller than the mean image intensity (mode<mean). In case the objects fill over 50% of the image area, the resulting binary image is inverted by default for final correct feature segmentation.

(3) The objects of interest are thought by default to be brighter than the background. For images which fulfill the opposite characteristics the mode value is most likely higher than the mean image intensity. For further processing, images which fulfill the latter characteristic will be simply inverted for the further processing to meet the criterion (2)  $\text{mode} < \text{mean}$ .

(4) Due to the assumptions (2) and (3) the mode will be most likely an intensity value which is present in the range of pixels to be finally assigned to the background in the binary image.

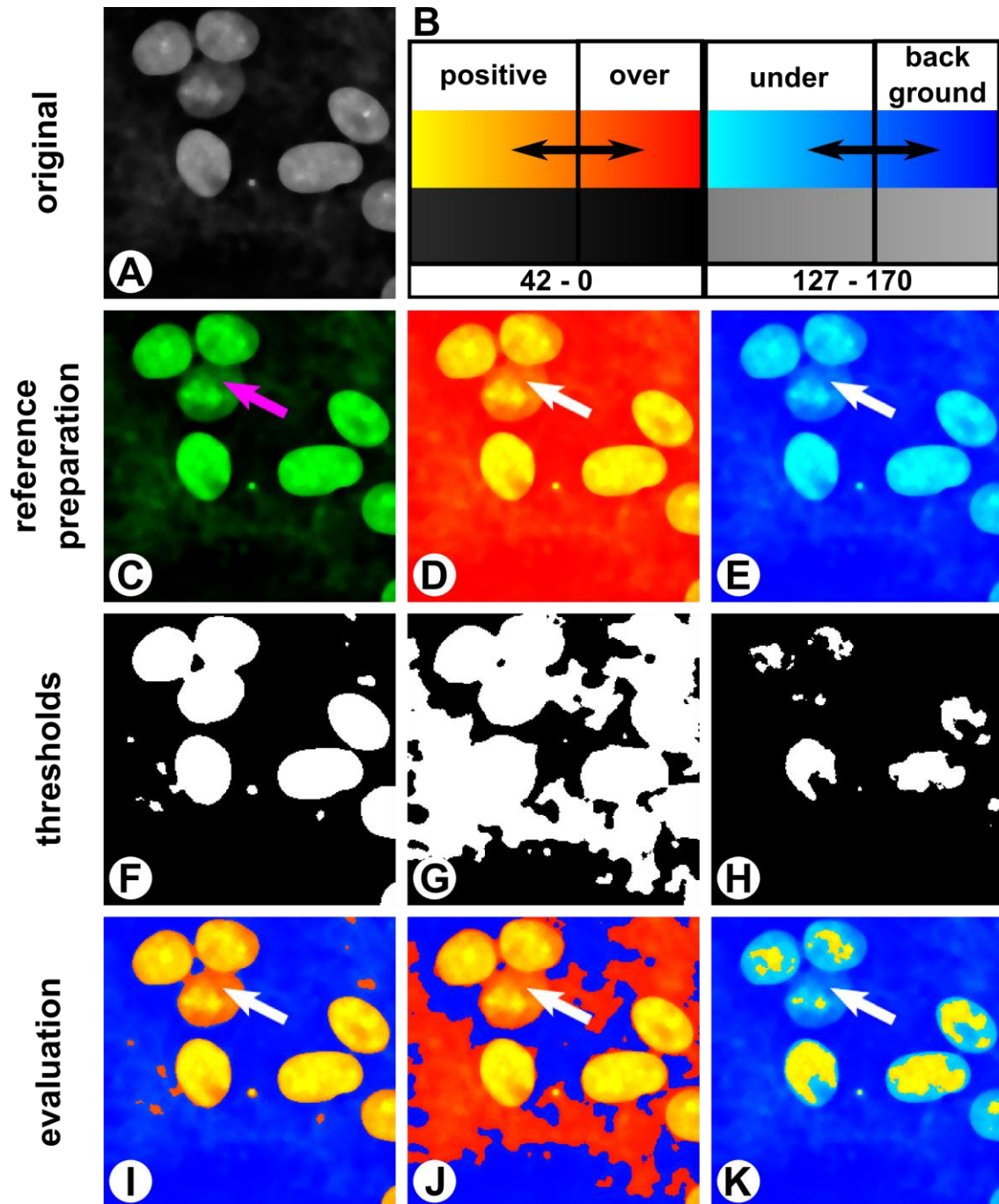


**FIGURE 1:** Qualitative and quantitative binarization evaluation procedure. (A) original image, (B) Image partitions scheme with assigned colors in RGB color space and the hue channel representation of HSB color space (gray scale below color representation) with the respective minimal and maximal pixel values assigned in the hue channel. (C) Pre-processed copy of original image, (D) reference image to determine cut-off value for separation of true positive pixels (yellow) from false positive (over-estimation, red) ones, (E) reference image to determine cut-off value for separation of true negative pixels (background, dark blue) from false negative (under-estimation, cyan) ones, (F-H) three different automatic binarization methods applied on the original image, (I-K) color-coded images for qualitative and quantitative evaluation of the different binarization methods shown in F-H. The arrow indicates the point selected for reference value determination. (l) shows an acceptable threshold, (J) an over-estimating and (K) and under-estimating threshold.

(5) If assumptions (2) - (4) are true, all values lying left of the mode (lower intensities) will finally be assigned to the background. Due to this fact, they might negatively influence the determination of some thresholds by shifting them towards the background intensities and away from the objects intensities. An elimination up to and including the mode intensity value initially limits the image content towards the intensities of the objects of interest and might thus further improve optimal threshold determination (see figure 2).

For the mode-limited mean (MoLiM) algorithm, a new mean value is calculated after initial intensity limitation from the restricted area which is then taken as the final threshold value.

In the case of the differential-limited mean (DiLiM) algorithm the initial limitation is done depending on the histogram context.

$$(Eq. 3) \quad T_{init} = \begin{cases} 1 - 255 \rightarrow \text{mean}^* - 255 & \text{if } \text{mode} = 0 \ \& \ \text{median} = 0 \\ \text{median} - 255 & \text{if } \text{mode} = 0 \ \& \ \text{median} > 0 \\ \text{median} - 255 & \text{if } \text{mode} > 0 \ \& \ |\text{mode} - \text{median}| < |\text{median} - \text{mean}| \\ \text{mode} - 255 & \text{if } \text{mode} > 0 \ \& \ |\text{mode} - \text{median}| > |\text{median} - \text{mean}| \end{cases}$$

mean\* = intermediate mean of the histogram range 1-255.

After this limitation to  $T_{init} - 255$  the new mean value is calculated as mentioned above and taken as the final threshold value before binarization. A comparison between a mean threshold and the MoLiM is schematically outlined in figure 2.

### 2.3 Test Images

The battery of test images for the evaluation of the mode-limited and differential-limited mean algorithm performance and the threshold evaluation method described above were chosen by including images with different histograms. In total 18 different images were evaluated. An excerpt of those test images is depicted in figure 3. The red arrows indicate the features of interest. The corresponding histograms are depicted next to or below the respective images.

### 2.4 Software

The method proposed here, makes use of the open source image processing and analysis software ImageJ [10] or Fiji [11] and its macro scripting language but could easily be transferred into a Java-plugin or using any other programming language. The decision to use the ImageJ software was also to make the evaluation method available for a big community of users without previous knowledge on the algorithms. The additional ease of using it inside ImageJ or Fiji is the presence of 16 global and 6 local automatic thresholding algorithms (at the time of manuscript preparation). Information and source code for the presented evaluation method can be downloaded and used in ImageJ or Fiji [12]–[14]. The two new binarization algorithms described here were implemented as an ImageJ/Fiji Java-plugin and will be publically available with publication of this manuscript as a Fiji update from the BioVoxel update inside the Fiji software [14].

For programming and evaluation of the algorithm Fiji with the ImageJ version 1.48f-h under Java 1.6.0\_24 [64-bit] was used. This version applied the AutoThreshold v1.15 from Gabriel Landini (19th February 2013) and the AutoLocal Threshold v1.4 from Gabriel Landini (2nd November 2011) [15], [16]. Three more local thresholds were available after manuscript preparation (updated on 18th November 2013) which were not included in this evaluation. Binarization was performed using the default settings for the local thresholding algorithms which were: radius = 15 pixels, parameter 1 = 0, and parameter 2 = 0.

### 2.5 Statistics

To compare the average performance quality measure of MoLiM and DiLiM an unpaired two-tailed student's t-test was performed due to variance homogeneity (determined using an F-test). The confidence interval was chosen at 95% ( $\alpha = 0.05$ ).

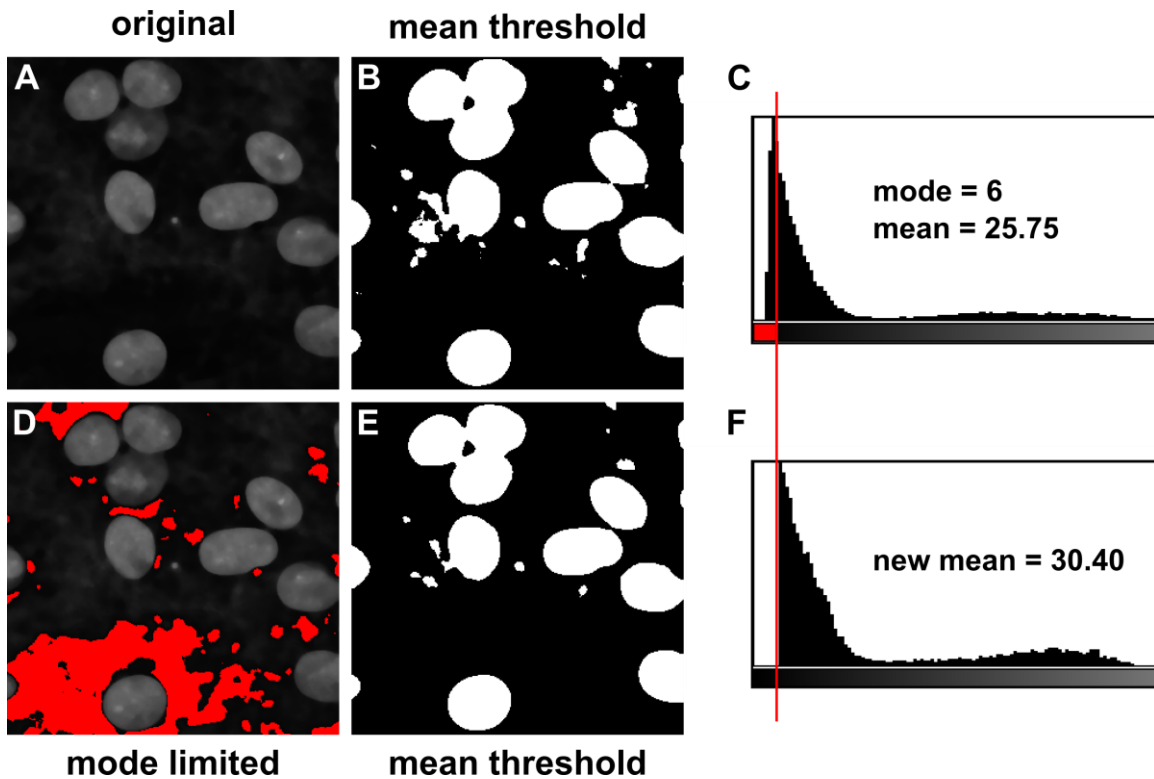


**FIGURE 2:** Outline of the mode limited mean algorithm. If the mean histogram value is taken as threshold on the original image (A) areas outside the wanted regions of interest are binarized (B). Initial limitation to the value above the mode value (7 in the example above) (C) excludes all pixels with a lower intensity value (D shown in red). This restricts the remaining image area and the histogram leading to an increase of the new histogram intensity mean (mode limited mean) and to a more specific binarization (E and F).

### 3. RESULTS

#### 3.1 Influence of Reference Point On Evaluation Output

First, the threshold quantification algorithm was checked for the influence of the reference point position and thus its intensity. Five different reference points were chosen in the same image as depicted in figure 4. The intensity differences in the selected point were as follows (TABLE 1):

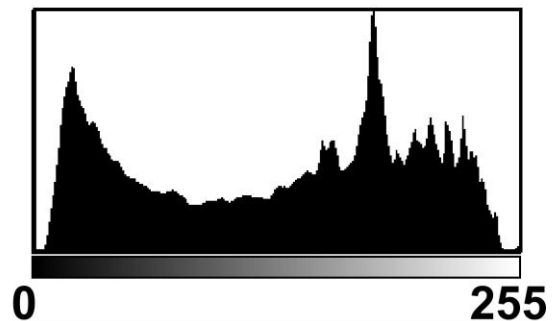
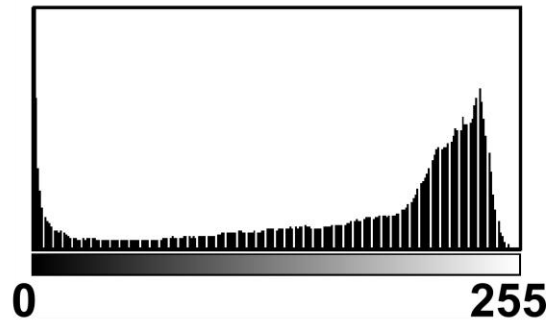
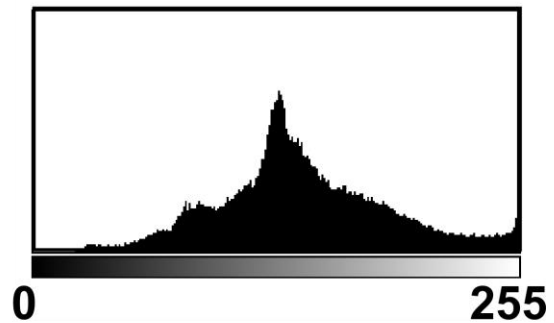
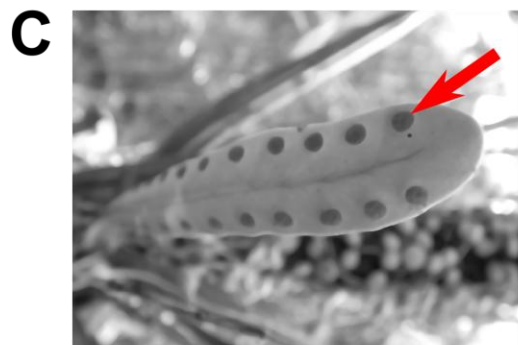
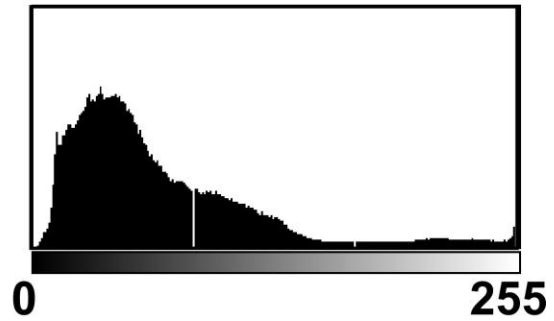
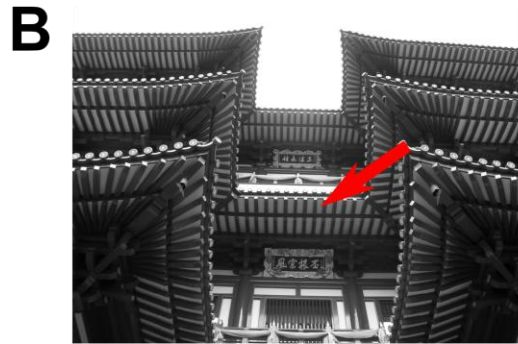
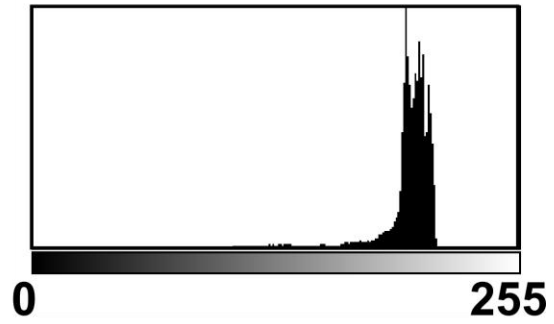
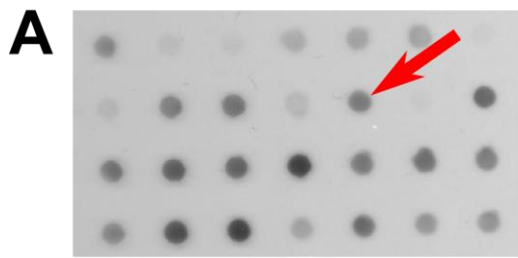
reference position	mean of reference pont	mean of 3x3 reference area
1	30	30.222
2	45	45.333
3	63	63.667
4	90	89.667
5	26	26.444

**TABLE 1:** Mean values of the reference point selection and the average intensity of the 3x3 area around the reference point.

#### 3.2 Robust High Performance of MoLiM and DiLiM Algorithms

The application of either the MoLiM or the DiLiM on 18 different test images revealed a good performance in feature extraction of both algorithms. Nine of those individual performance analyses are shown in figure 5. In 2 out of the 18 cases MoLiM performed better than all other methods (on images: 'Chillis' and 'Muscle'). The performance of MoLiM and DiLiM was above the average performance of all methods for the individual images with the exception of one image in the case of MoLiM and 3 images for DiLiM. Both methods also were performing superior than the over-all cumulative performance quality for the complete set (all methods tested on all test images) of 62.82%. None of the local thresholds had an average performance better than the over-all performance quality. The global thresholds "Minimum", "Percentile" and "Shanbhag" also performed worse than this limit. The best thresholds in the current test set besides MoLiM was "RenyiEntropy" and "Li". MoLiM had a tendency to give the best binarization results under the chosen conditions while this was not significant for all comparisons as shown in figure 6. The latter indicates that both, MoLiM and DiLiM, performed significantly better than all the local thresholds as well as the global thresholds "Percentile" and "Shanbhag". MoLiM was further superior to "Intermodes", "MinError" and "Minimum".

Thus, in the context of specific feature extraction, the MoLiM and DiLiM algorithm can be considered to be a robust binarization method over a wide range of different digital images and histogram shapes.



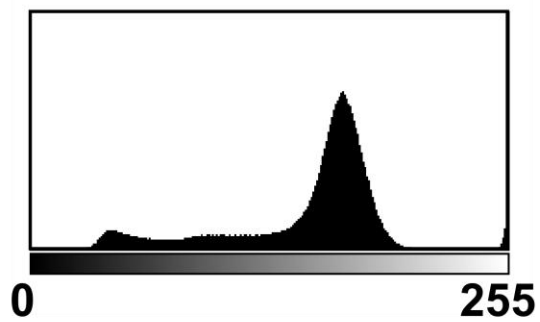
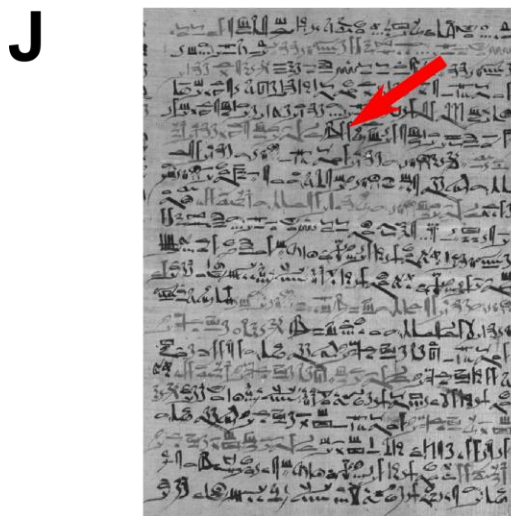
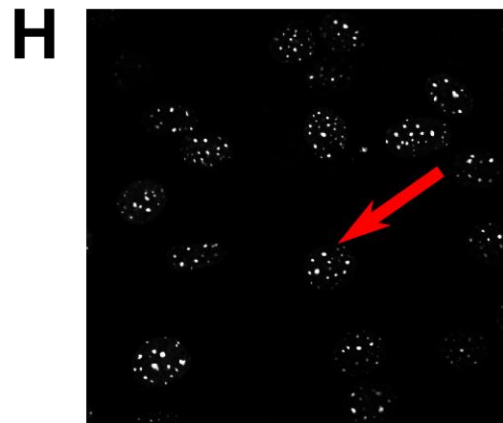
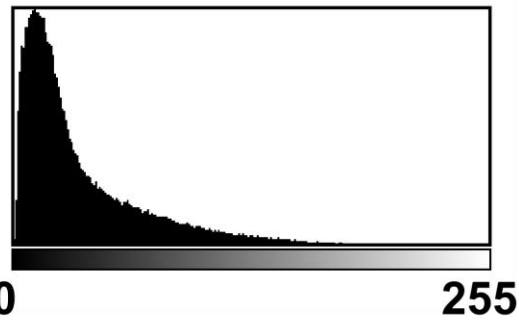
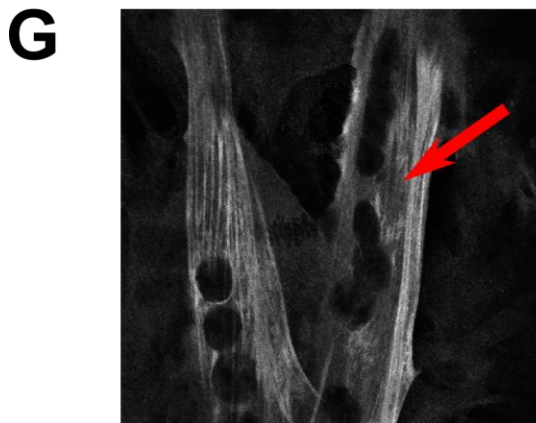
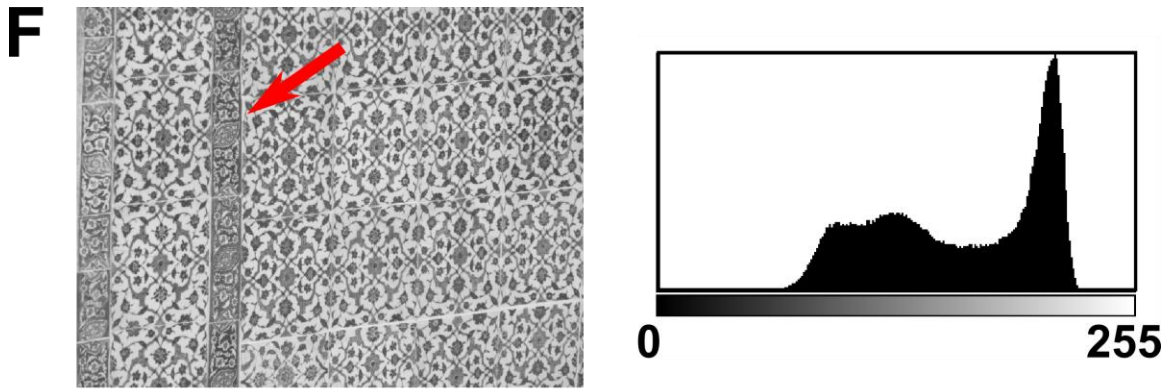


**FIGURE 3:** Excerpt of test images to investigate the performance of the "mode limited mean" and "differential limited mean" algorithms. Images were chosen to reflect different histogram shape distributions to account for a variety of images where binarization might be applied, such as landscapes, natural scenes (B-E), patterns (F), biological images (A, G and H), and text documents (J, [17]). The corresponding histograms are depicted on the right hand side or below the respective images.

As expected, the reference point selection showed an influence on the evaluation and thus also on the suggestion of the respective threshold to be considered the best. The thresholds performing with a similar qualitative appearance and quantitative value (Li and MaxEntropy in figure 3B and F) obviously are those with reference mean intensity values lying close together.

This indicates, that the choice of the intensity reference cut-off value needs to be done very thoroughly to retrieve reliable results. Additionally, the quantitative results need to be seen in the context of the qualitative visual output in the color-coded images as well as the analytical context in which the images will be analyzed. This also permits the influence of the user which thus can figure out thresholds fulfilling his/her needs apart from pure intensity separation quality.

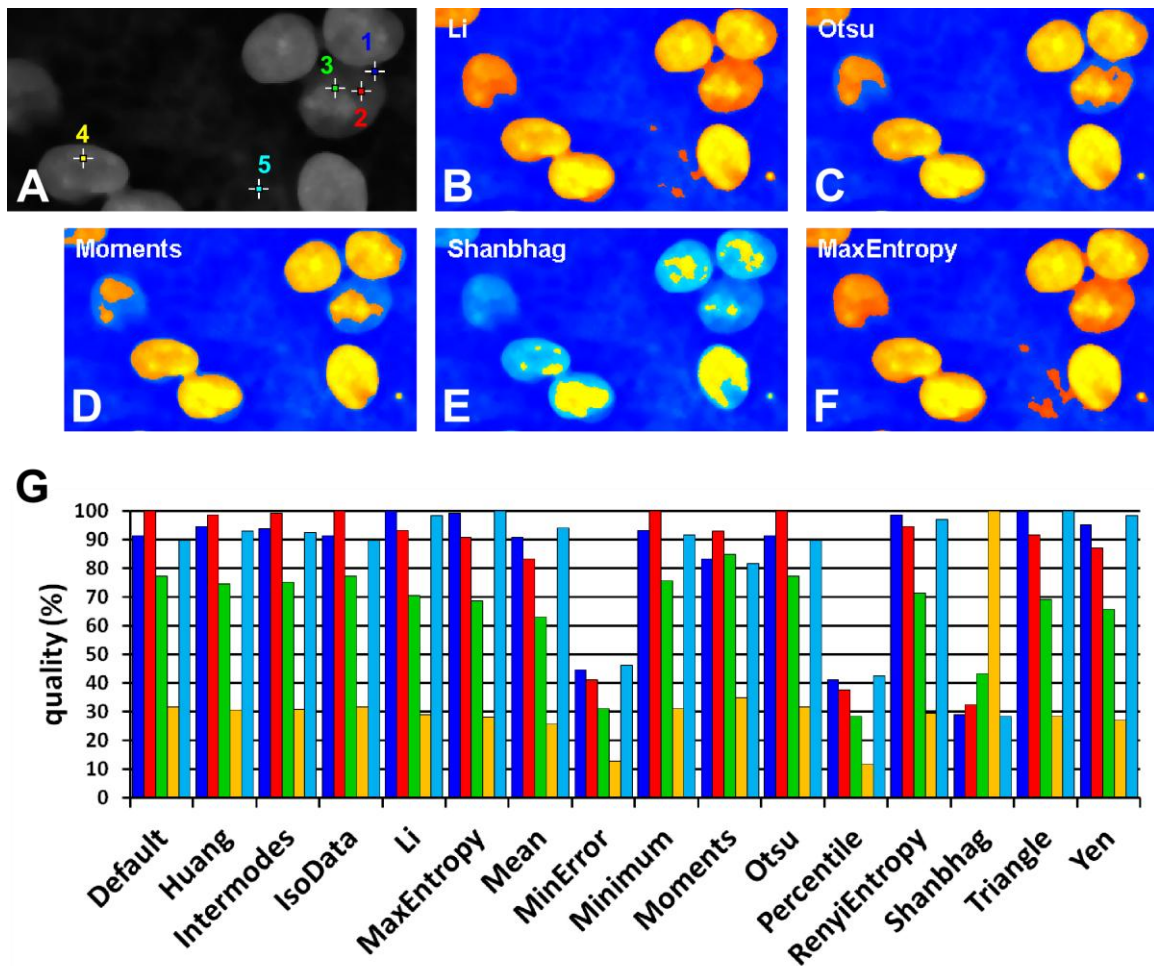


**FIGURE 4:** Influence of reference point position on evaluation results. (A) indication of reference point position. (B-F) Thresholds quantified as the best thresholds relative to the reference point selection: (B) reference point 1, threshold: Li, (B) reference point 2, threshold: Otsu, (B) reference point 3, threshold: Moments, (B) reference point 4, threshold: Shanbhag, (B) reference point 5, threshold: MaxEntropy. (G) Graph showing the relative quality measure in percentage in relation to the reference point selections (indicated by the same colors).

## 4. DISCUSSION

### 4.1 Semi-automatic Quantitative and Qualitative Binarization Evaluation

Objective evaluation of binarization techniques is a difficult task, since specific reference criteria need to be set fixed beforehand or need to be calculated from the original image content itself in a way which enables realistic quality assessment. User-specific requirements on the extracted objects further make this more difficult. Besides the advantage of unsupervised binarization analysis, methods with either fixed quality reference parameters or those applying machine learning algorithms on representative images might suffer from a decrease in reliability depending on several factors. Those include an increasing variability in image content or intensities as well as contrast differences in a series of images to be evaluated together or difficult automatic shape or edge determination of objects.

The method presented here does not apply complete unsupervised analysis but allows an easy and quick evaluation of several binarization methods for untrained users. Obviously, a certain user bias is unavoidable and the reliability of the quantitative output relates to the carefulness during reference intensity cut-off value selection. It should also be mentioned that the method could in theory be implemented as unsupervised batch processing procedure with a fixed reference intensity value given as delineation criteria. Of importance is that comparison of all binarization algorithms present in the respective implementation is done in relation to the very same, previously chosen reference value and thus represents an unbiased evaluation of different binarization results from the same original image. In general, it is less biased and superior to manual threshold definition as well as to simple visual comparison of the binary results of several automatic segmentations with the original image counterparts.

The current literature contains several reports on different evaluation methods regarding image segmentation in general, while many of those deal with multi-class segmentation algorithms such as "Mean Shift", other statistical region merging methods which are mostly applied to color images [8], [18]–[21]. Those analyses are unequally more difficult compared to the problem discussed here. This originates from the fact that the classification into different regions which in the best case resemble separated real objects is a difficult task itself while the individual perception on those might additionally be highly variable. Thus, a decision on the correct or incorrect pixel classification needs to include many different criteria such as intra- as well as inter-region variances (e.g. by using entropy calculations) [19]. Of note, while the present report rather deals with the separation of information into 2 classes only, including techniques of regional combination as pre-processing step in grayscale images might in turn improve the object separation during binarization. Ge and coauthors present evaluations according to the extraction of the most salient object in the image [22] which is not necessarily possible by separation of intensities above a certain threshold from those below as mostly aimed for during binarization. Therefore, such a method needs to consider different image properties regarding reliable segmentation events. Most publications evaluating binarization algorithms do this in the limited context of document binarization and thus text extraction [3], [23]–[25] which in comparison to the above mentioned methods as well as the use of natural or biological images might show a rather low complexity. One of those reports compared binarization results of synthetically created images with their corresponding original counterparts [3] which makes the evaluation during a test setup less error prone but is not transferable to real life examples. This applicability to real images was an important prerequisite during the development of the proposed method. The presented evaluation is independent of the image context and only limited to the intensity distribution in grayscale images.

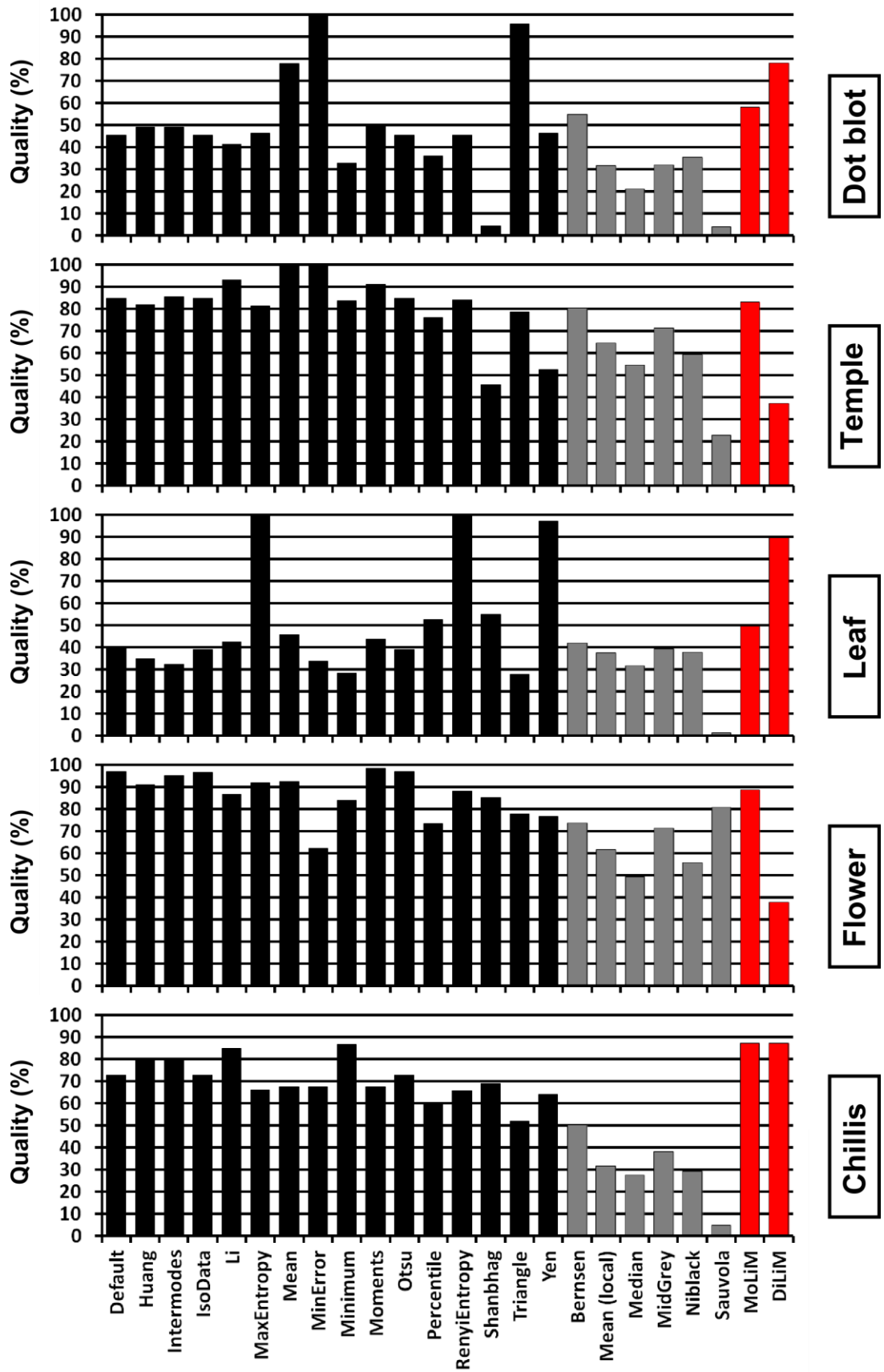
Furthermore, available methods often rely on the comparison of the binarization result with one or more ground-truth images mostly retrieved by previous manual segmentation [22], [26]. This makes the procedure time intensive and needs one or more experts to create more or less reliable ground truth samples. Moreover, those examples not necessarily present the best basis for comparison in a context with high inter-image variability. Different unsupervised methods compare regions to e.g. edge maps determined by edge finding algorithms [21] and thus strongly rely on the performance quality of those techniques.

The proposed method takes the original image information as the best and unaltered ground truth which perfectly accounts for the different intra- as well as inter-image variability in addition. Hence, there is no time consuming search or biased creation of ground truth segmentations necessary which as mentioned naturally neglect a certain amount of variability during comparison. Nevertheless, the reference intensity cut-off needs to be chosen in the described method individually which, without a doubt, includes a certain amount of user bias as well. Besides this, a basically infinite amount of known binarization algorithms can be compared straight forward based on the same reference point and as such the proposed method represents a quick, robust and reliable, quantitative measure for relative binarization quality assessment for individual images.

The described comparison of binarization methods also might highlight certain limitations of a pool of automatic segmentation algorithms regarding a specific image when reaching relative qualities markedly below 100% as well as non-satisfying visual output. The latter might directly indicate that a complete or partial feature extraction in the current image under the chosen conditions might not be achievable without further image pre-processing (e.g. filtering) or image improvement and thus saves time by avoiding a trial and error adjustment e.g. using manual thresholds.

Therefore, a thorough selection of the reference value is crucial for the performance of the quantitative evaluation. The reference point has to be positioned as close as possible to the intensity value which should still be recognized (darkest value to be accepted for bright objects and brightest value to be accepted for dark objects) and extracted.

In summary, the described algorithm is based on a qualitative output for visual analysis of color-coded images and a numerical quantification of the binarization performance. In combination, both output formats provide an easy evaluation method to test the quality of individual image segmentations and reliably compare them to each other under set conditions. This is especially useful to determine the best segmentation algorithm when several of them perform visually similar. Then, the quantitative evaluation might point out slight superior binarization performances not visually determinable by the user in the context of the reference point selection.



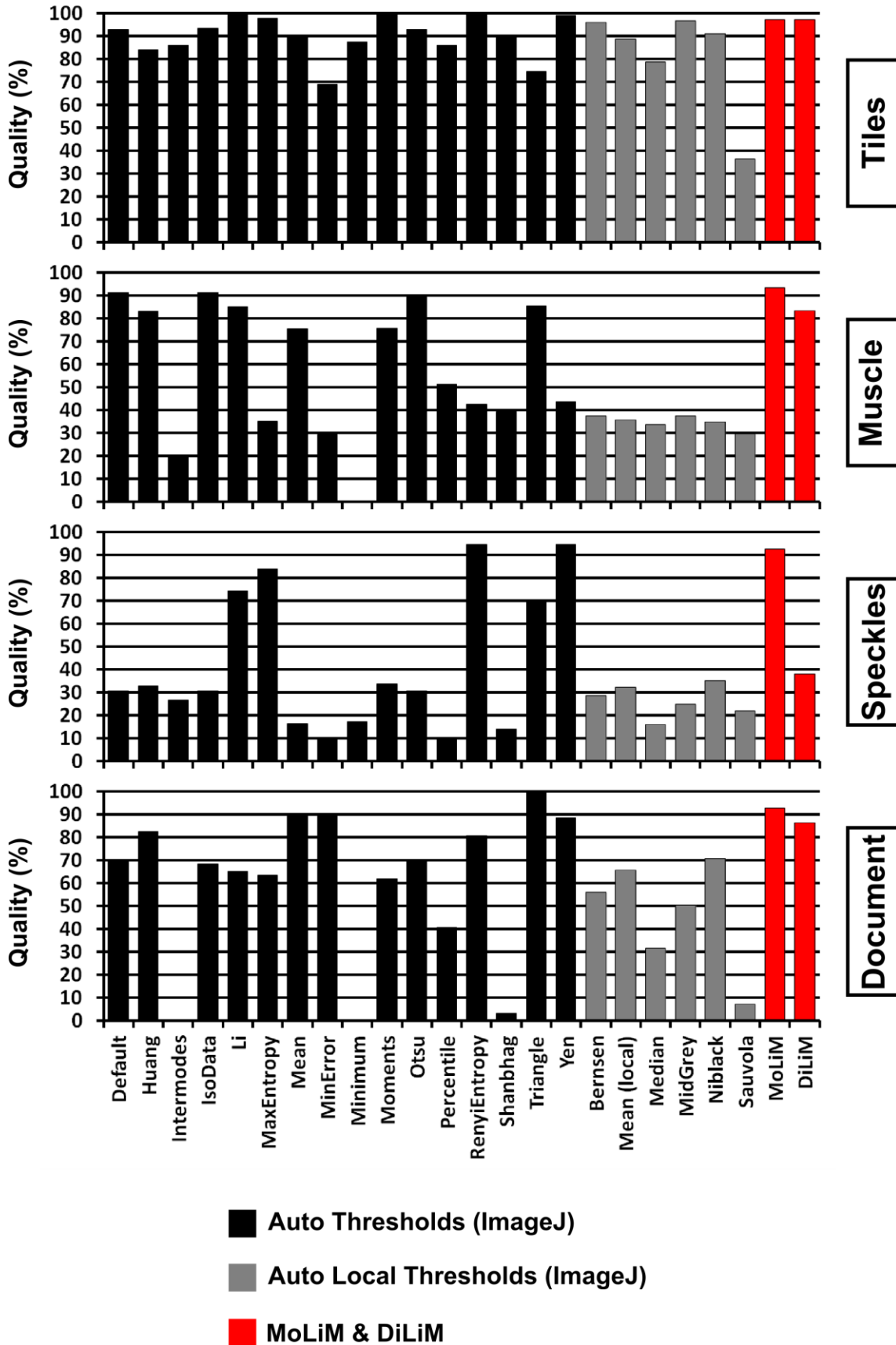


**FIGURE 5:** Exemplary performance evaluations of nine test images using the "Threshold Check" proposed above. Quality output is shown in percent (%) relative to the chosen intensity reference cut-off value. Black columns represent ImageJ AutoThreshold methods, gray columns the Auto Local Thresholds implemented in ImageJ and red columns indicate the newly proposed methods MoLiM and DiLiM. The graphs correspond to the test images depicted in figure 3.

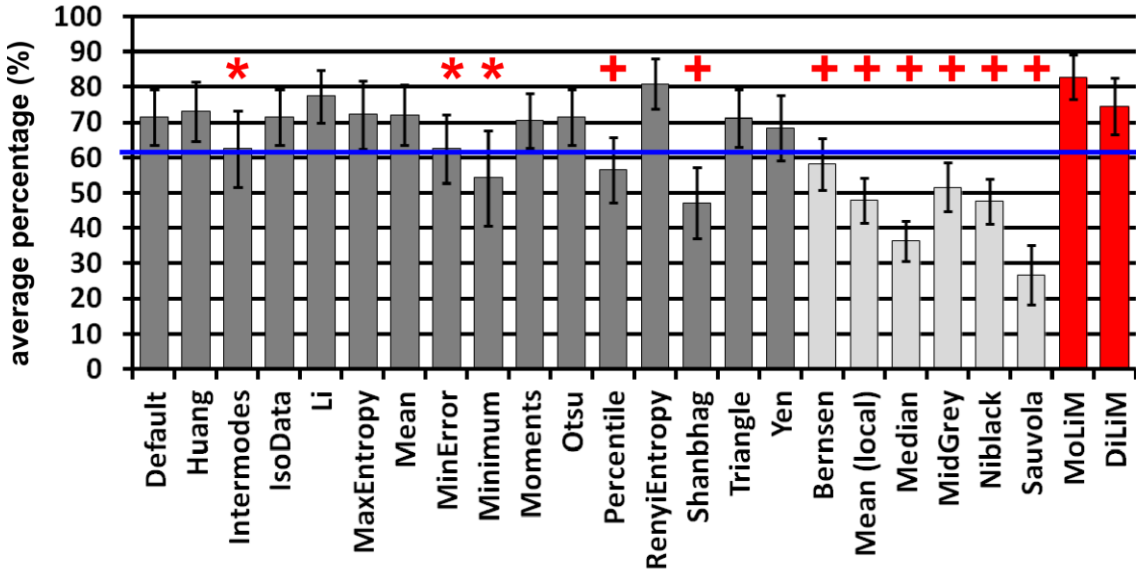


**FIGURE 6:** Average performance evaluation of MoLiM and DiLiM algorithms (red) in comparison with 16 established global (dark gray) and 6 local (light gray) automatic binarization methods. Depicted is the individual average relative quality measure in percent using n=18 test images with different histogram appearances. Error bars indicate the standard error of the mean (S.E.M.). The blue line indicates the average performance calculated from all auto threshold algorithms over all tested images together. Asterisks indicate significant better performance of the MoLiM, while crosses indicates a significantly better performance of both, MoLiM and DiLiM, in comparison to the indicated methods. Significance was accepted for p-values <0.05.

#### 4.2 MoLiM and DiLiM Performance

The newly proposed binarization algorithms MoLiM and DiLiM use an initial limitation of the histogram and the respective image area according to the histograms mode or median value and hence achieve a good separation of potential background from foreground (region of interest) pixels.

The method tested here included a low precision hue value determination assigning one hue value to six consecutive colors in RGB color space. Nevertheless, the application of a high precision hue value determination in the reference and test images had only little influence on the relative quality assessment of the individual thresholds (data not shown). Besides that, they resulted in a considerable drop of the algorithms' time performance in the current test setup. This performance decreased strongly with increasing image size. In this case, processing time strongly out-performed precision. Furthermore, the slight reduction in precision might improve the robustness regarding the intensity reference point selection, since individual pixel differences will have a reduced impact on the evaluation.

The advantage of the proposed algorithm is that it does not depend on the histogram shape such as the existence of two mode values (peaks) [27], a fixed percentage of foreground pixels [28] or the necessity to iteratively converge two threshold values [29]. Thus, besides being computationally efficient, the algorithm never fails to achieve a binarization.

MoLiM significantly out-performed 11 and DiLiM 8 out of 22 tested binarization algorithms under the chosen test conditions and in respect to the relative reference point. The latter was chosen as

objective as possible to indicate a cut-off value which leads to good separation of the objects of interest in the individual images from the supposed background.

## 5. CONCLUSION

The semi-automatic segmentation performance evaluation presented here can be applied to all types of binarization algorithms as long as the original image is available. Furthermore, a set of automatic binarization methods can be included directly before the analysis as implemented in an ImageJ macro script prepared to produce the results described in this manuscript. This makes the evaluation process extremely time efficient. It is easy to use and simply implies some knowledge about the objects of interest and the requirements for further analyses.

The MoLiM and DiLiM binarization algorithms evaluated with the described quality assessment provided very robust and computationally low-cost segmentation results as alternatives to many other existing thresholding methods.

## 6. FUTURE DIRECTIONS

Besides the fact of the often stated importance of such segmentation evaluation techniques there is only a limited number available so far which still holds potential for future related research. The presented method will be tested for application in a batch processing setup to see if, besides comparison of several binarization algorithms using one image, a reliable and robust comparison can also be achieved when comparing a set of similar images. Therefore, a fixed reference value as ground truth criteria needs to be chosen. The studies will include trials on reference intensity choices according to intra-image intensity distribution and inter-image intensity fluctuations.

## 7. REFERENCES

- [1] P. . Sahoo, S. Soltani, and a. K. . Wong, "A survey of thresholding techniques," *Comput. Vision, Graph. Image Process.*, vol. 41, no. 2, pp. 233–260, Feb. 1988.
- [2] C. A. Glasbey, "An Analysis of Histogram-Based Thresholding Algorithms," *CVGIP: Graphical Models and Image Processing*, vol. 55, no. 6. pp. 532–537, 1993.
- [3] P. Stathis and N. Papamarkos, "An Evaluation Technique for Binarization Algorithms," vol. 14, no. 18, pp. 3011–3030, 2008.
- [4] R. Unnikrishnan, C. Pantofaru, and M. Hebert, "A Measure for Objective Evaluation of Image Segmentation Algorithms," in *2005 IEEE Computer Society Conference on Computer Vision and Pattern Recognition (CVPR'05) - Workshops*, vol. 3, pp. 34–34.
- [5] J. S. Weszka and A. Rosenfeld, "Threshold Evaluation Techniques," *IEEE Trans. Syst. Man. Cybern.*, vol. 8, no. 8, pp. 622–629, Aug. 1978.
- [6] A. Najjar and E. Zagrouba, "An Unsupervised Evaluation Measure of Image Segmentation : Application to Flower Image," pp. 448–457, 2012.
- [7] H. Zhang, S. Cholleti, S. A. Goldman, and J. E. Fritts, "Meta-Evaluation of Image Segmentation Using Machine Learning," in *EEE Computer Society Conference on Computer Vision and Pattern Recognition - Volume 1 (CVPR'06)*, vol. 1, pp. 1138–1145.
- [8] M. Borsotti, P. Campadelli, and R. Schettini, "Quantitative evaluation of color image segmentation results," *Pattern Recognit. Lett.*, vol. 19, no. 8, pp. 741–747, 1998.

- [9] J. A. Shufelt, "Performance evaluation and analysis of monocular building extraction from aerial imagery," *IEEE Trans. Pattern Anal. Mach. Intell.*, vol. 21, no. 4, pp. 311–326, Apr. 1999.
- [10] C. A. Schneider, W. S. Rasband, and K. W. Eliceiri, "NIH Image to ImageJ: 25 years of image analysis," *Nat. Methods*, vol. 9, no. 7, pp. 671–675, Jun. 2012.
- [11] J. Schindelin, I. Arganda-Carreras, E. Frise, V. Kaynig, M. Longair, T. Pietzsch, S. Preibisch, C. Rueden, S. Saalfeld, B. Schmid, J.-Y. Tinevez, D. J. White, V. Hartenstein, K. Eliceiri, P. Tomancak, and A. Cardona, "Fiji: an open-source platform for biological-image analysis.," *Nat. Methods*, vol. 9, no. 7, pp. 676–82, Jul. 2012.
- [12] J. Brocher, "BioVoxel Toolbox," 2014. [Online]. Available: [http://fiji.sc/BioVoxel\\_Toolbox](http://fiji.sc/BioVoxel_Toolbox). [Accessed: 05-Mar-2014].
- [13] J. Brocher, "Theshold Check (BioVoxel Toolbox)," 2014. [Online]. Available: [http://fiji.sc/BioVoxel\\_Toolbox#Threshold\\_Check](http://fiji.sc/BioVoxel_Toolbox#Threshold_Check). [Accessed: 05-Mar-2014].
- [14] J. Brocher, "BioVoxel Fiji update site," 2014. [Online]. Available: <http://sites.imagej.net/BioVoxel/>. [Accessed: 05-Mar-2014].
- [15] G. Landini, "Auto Thresholds," 2013. [Online]. Available: [http://fiji.sc/wiki/index.php/Auto\\_Threshold](http://fiji.sc/wiki/index.php/Auto_Threshold). [Accessed: 29-Nov-2013].
- [16] G. Landini, "Auto Local Thresholds," 2013. [Online]. Available: [http://fiji.sc/Auto\\_Local\\_Threshold](http://fiji.sc/Auto_Local_Threshold). [Accessed: 29-Nov-2013].
- [17] "Edwin Smith Papyrus." [Online]. Available: [http://upload.wikimedia.org/wikipedia/commons/b/b4/Edwin\\_Smith\\_Papyrus\\_v2.jpg](http://upload.wikimedia.org/wikipedia/commons/b/b4/Edwin_Smith_Papyrus_v2.jpg). [Accessed: 24-Jan-2014].
- [18] H. Zhang, J. E. Fritts, and S. a. Goldman, "Image segmentation evaluation: A survey of unsupervised methods," *Comput. Vis. Image Underst.*, vol. 110, no. 2, pp. 260–280, May 2008.
- [19] H. Zhang, J. E. Fritts, and S. a. Goldman, "An entropy-based objective evaluation method for image segmentation," no. 1, pp. 38–49, Dec. 2003.
- [20] R. Unnikrishnan, C. Pantofaru, and M. Hebert, "Toward objective evaluation of image segmentation algorithms.," *IEEE Trans. Pattern Anal. Mach. Intell.*, vol. 29, no. 6, pp. 929–44, Jun. 2007.
- [21] J. Freixenet, X. Mu, D. Raba, J. Mart, and X. Cuf, "Yet Another Survey on Image Segmentation : Region and Boundary Information Integration," *ECCV*, pp. 408–422, 2002.
- [22] F. Ge, S. Wang, and T. Liu, "Image-Segmentation Evaluation From the Perspective of Salient Object Extraction," *2006 IEEE Comput. Soc. Conf. Comput. Vis. Pattern Recognit. - Vol. 1*, vol. 1, pp. 1146–1153, 2006.
- [23] O. D. Trier and T. Taxt, "Evaluation of binarization methods for document images," *IEEE Trans. Pattern Anal. Mach. Intell.*, vol. 17, no. 3, pp. 312–315, Mar. 1995.

- [24] A. Kefali, T. Sari, and M. Sellami, "Evaluation of several binarization techniques for old Arabic documents images," in *The First International Symposium on Modeling and Implementing Complex Systems MISC*, 2010, no. 1, pp. 88–99.
- [25] K. Ntirogiannis, B. Gatos, and I. Pratikakis, "An Objective Evaluation Methodology for Document Image Binarization Techniques," in *2008 The Eighth IAPR International Workshop on Document Analysis Systems*, 2008, pp. 217–224.
- [26] J. K. Udupa, V. R. LeBlanc, Y. Zhuge, C. Imielinska, H. Schmidt, L. M. Currie, B. E. Hirsch, and J. Woodburn, "A framework for evaluating image segmentation algorithms," *Comput. Med. Imaging Graph.*, vol. 30, no. 2, pp. 75–87, Mar. 2006.
- [27] J. M. S. Prewitt and M. L. Mendelsohn, "THE ANALYSIS OF CELL IMAGES\*," *Ann. N. Y. Acad. Sci.*, vol. 128, no. 3, pp. 1035–1053, Dec. 2006.
- [28] W. Doyle, "Operations Useful for Similarity-Invariant Pattern Recognition," *J. ACM*, vol. 9, no. 2, pp. 259–267, Apr. 1962.
- [29] J. Kittler and J. Illingworth, "Minimum error thresholding," *Pattern Recognit.*, vol. 19, no. 1, pp. 41–47, Jan. 1986.

## Comparative Performance of Image Scrambling in Transform Domain using Sinusoidal Transforms

### H.B.Kekre

*Sr. Professor, Computer Engg.  
MPSTME, NMIMS University  
Mumbai, 400056, India*

*hbkekre@yahoo.com*

### Tanuja Sarode

*Associate. Professor, Computer Engg.  
TSEC, Mumbai University  
Mumbai, 400050, India*

*tanuja\_0123@yahoo.com*

### Pallavi N. Halarnkar

*PhD. Research Scholar  
MPSTME, NMIMS University  
Mumbai, 400056, India*

*pallavi.halarnkar@gmail.com*

### Debkanya Mazumder

*Student, Computer Engg.  
MPSTME, NMIMS University  
Mumbai, 400056, India*

*rimjhim.mazumder17@gmail.com*

---

### Abstract

With the rapid development of technology, and the popularization of internet, communication is been greatly promoted. The communication is not limited only to information but also includes multimedia information like digital Images. Therefore, the security of digital images has become a very important and practical issue, and appropriate security technology is used for those digital images containing confidential or private information especially. In this paper a novel approach of Image scrambling has been proposed which includes both spatial as well as Transform domain. Experimental results prove that correlation obtained in scrambled images is much lesser then the one obtained in transformed images.

**Keywords:** Scrambling, Key Based Scrambling, Sinusoidal Transforms, DCT, DST, DFT, Real Fourier, Discrete Hartley.

---

## 1. INTRODUCTION

Traditional permutation encryption algorithm is not robustness for noise disturbing and shear transformation attacks. An Image encryption algorithm is introduced based on location transformation in [1]. The method is robust against noise and shear transformation attacks which is the advantage over traditional encryption algorithms. The algorithm encrypts the image based on chaotic system and stores the pixel values in multiple places. A variation of extended magic square matrix generating algorithm is also presented. The variation has a good efficiency over the traditional magic square matrix generation algorithm. Experimental results show a good improvement when encrypted image is modified with noise and shear transformation attack.

The unique property of chaotic functions gives its way to Image Encryption. A new combined technique is given in [2] which has better chaotic behavior than the traditional ones. The technique involves the concept of confusion and diffusion in encryption of Digital images. The experimental results show that the method has a higher security level and excellent performance.

Chaotic sequences ranking is used as a base for encryption algorithm and the technique is presented in [3]. The method is aimed at the deficiency of the existing color image encryption method. As the first step the scrambling algorithm scrambles the positions of color image and sets one to one relationship between the image matrix and chaotic sequence. In the next step the row and column of the image matrix ranking were guided by the chaotic sequence ranking. In order to improve the security, the pixel values of the scrambled color image is shuffled. The shuffling is based on the chaotic sequence ranking. Overall the method has a good encryption effect.

An image encryption is proposed in [4] which is based on logistic map and hyper-chaos. The logistic map is used to generate the chaotic key 1 which has a good randomness. The Hyperchaos system is used to produce the chaotic key2. Encryption algorithm has two rounds each with the two different keys generated with two different chaotic maps. The experimental results show that the method has good results, high efficiency, good statistical characteristics and differential characteristics

Using the Baker map, an image encryption algorithm is presented in [5]. The proposed method makes use of discrete cosine transform (DCT), the discrete sine transform (DST), the discrete wavelet transform (DWT) and the additive wavelet transform (AWT) for Image encryption approach. Chaotic encryption is performed in these transform domains to make use of the characteristics of each domain. Different attacks are studied for all the transforms used for encryption. DST transform gives good results compared to others if degree of randomness is of major concern.

An image encryption algorithm is implemented in transform domain using DWT and stream ciphers. A stream cipher helps to make information (plain text) into an unreadable format. A comparative study on DCT and DWT is also discussed in [6].

A novel approach of Image encryption is proposed in [7], it transforms an encrypted original image into another image which is the final encrypted image and same as the cover image overcoming the drawback of transmitting the noise like image over the network and making it suspicious for intruders. The proposed algorithm is based on Wavelet decomposition. Experimental results show simulation and security analysis results

An extended version of TJ-ACA: advanced cryptographic algorithm is been proposed named as TJ SCA: supplementary cryptographic algorithm for color images in [8]. A white blank image whose preview is not available in transform domain is generated, which makes the brute force attacks ineffective. The proposed method makes use of 2-D fast Fourier transform, ikeda mapping are used to get a highly secured image. The method also gives a Lossless decryption. Therefore the method is applicable to stego images.

A new encryption algorithm based on bit plane decomposition to improve the security level is introduced in [9]. The technique combines parametric bit plane decomposition, bit plane shuffling, resizing, pixel scrambling and data mapping techniques for encryption. For bit plane decomposition, Fibonacci P-code is used and 2D P-Fibonacci is used for image encryption. Experimental result shows the ability of the method against several common attacks. The method can be used to encrypt images, biometrics and videos.

An extension to ScaScra is proposed in [10]. It is used to scramble a digital image in the diagonal direction. The diagonal blocks are first decided, the pixels in these blocks are scrambled using unified constructive permutation function. The scrambling technique is scalable by varying the block size. Subjective and objective experiments were carried out to test the performance of the proposed technique and the results were compared to ScaScra. Experimental parameters like correlation and entropy were used.

An optical information hiding technique for digital images is proposed in [11]. The technique combines the scrambling technique in fractional Fourier domain. Firstly image is randomly shifted using the jigsaw transform algorithm and then a scrambling technique based on Arnold transform is applied. Then the image is iteratively scrambled in fractional Fourier domains using randomly chosen fractional orders. The parameters of the jigsaw transform, Arnold and fractional Fourier forms a huge key space and thus resulting in high security of the proposed encryption method. Experimental results demonstrate the flexibility and robustness of the proposed method.

In [12] the periodicity of scrambling process is analyzed using Arnold transformation to get some universal rules, then improved intersecting cortical Model Neural Network (ICMNN) is used to extract 1D signatures of the original image and scrambled images which reflects the image structure changing process. L1 norm is been adopted to evaluate the scrambling degree and the universal rules obtained above are used to verify the results. The experimental results showed that the proposed method could analyze and evaluate the scrambling degree efficiently.

A symmetric encryption algorithm based on bit permutation, using an iterative process combined with chaotic function is proposed in [13]. The advantage of this technique is secured encryption and getting confusion and diffusion and distinguishability properties in the cipher. The output of the cryptosystem is measured based on the statistical analysis of randomness, sensitivity and correlation on the cipher-images.

Information security and confidentiality is important at different levels of communication. The applications find their way into different fields like personal data, patient's medical data, military etc. With the advancement in Research in the field of Image processing, Image encryption and steganographic techniques have gained a popularity over the other forms of hidden communication. A new Image Encryption technique using Fibonacci and Lucas is proposed in [14]. The approach makes use of Arnold Transform matrix, and uses the generalized Fibonacci and lucas series values in the Arnold transform to scramble the image.

An encryption technique based on pixels is proposed in [15]. Firstly the image is scrambled using the method of watermarking making it difficult for decoding purpose. Lastly a camouflaged image to vision or the pixels of the true image to get the final encrypted image. The key parameters are encrypted using Elliptic curve cryptography (ECC). The algorithm security, reliability and efficiency is analyzed via experimental analysis.

A new invertible two dimensional map is proposed in [16] called as Line Map, for image encryption and decryption. The method maps the digital image to an array of pixels and then maps it back from array to image. A Line Map consists of two maps, a left map and a right map. The drawback of the traditional 2D maps which can be used only for permutation is overcome by Line Map which can perform two processes of image encryption, permutation and substitution simultaneously using the same maps. The proposed method does not have a loss of information, it is also fast and there is no restriction on the length of the security key.

Non Sinusoidal Transforms, such as Walsh, Slant, Kekre and Haar have been tried for this approach in [19]. Experimental results have shown Kekre transform performs better than all other Non Sinusoidal Transforms. In this paper, we are exploring Sinusoidal Transforms such as DCT, DST, Real Fourier, Hartley and DFT.

## **2. SINUSOIDAL TRANSFORMS**

A Transform is a technique for converting a signal into elementary frequency components. Transform coding relies on the premise that pixels in an image exhibit a certain level of correlation with their neighboring pixels. Consequently, these correlations can be exploited to predict the value of a pixel from its respective neighbors. A sinusoidal unitary transform is an invertible linear transform whose kernel describes a set of complete, orthogonal discrete cosine and/or sine basis functions

### 2.1 Discrete Cosine Transform

A Discrete Cosine Transform (DCT) expresses a sequence of finitely many data points in terms of a sum of cosine functions oscillating at different frequencies. DCTs are important to numerous applications in science and engineering, from lossy compression of audio and images (where small high-frequency components can be discarded), to spectral methods for the numerical solution of partial differential equations. The use of cosine rather than sine functions is critical in these applications: for compression, it turns out that cosine functions are much more efficient, whereas for differential equations the cosines express a particular choice of boundary conditions.

The DCT can be written as the product of a vector (the input list) and the  $n \times n$  orthogonal matrix whose rows are the basis Vectors. We can find that the matrix is orthogonal and each basis vector corresponds to a sinusoid of a certain frequency. The general equation for a 2D (N data items) is given below

$$F(m, n) = \frac{2}{\sqrt{MN}} C(m)C(n) \sum_{x=0}^{M-1} \sum_{y=0}^{N-1} f(x, y) \cos \frac{(2x+1)m\pi}{2M} \cos \frac{(2y+1)n\pi}{2N} \quad (1)$$

Where  $C(m), C(n) = 1/\sqrt{2}$  for  $m, n=0$  and  $C(m), C(n)=1$  otherwise

### 2.2 Discrete Sine Transform

The Discrete Sine Transform (DST) is a member of sinusoidal unitary transforms family. DST is real, symmetric, and orthogonal. It is used as an alternative transform in Transform Coding system. The general equation for a 2D (N data items) is given below.

$$\varphi(k, n) = \sqrt{\frac{2}{N+1}} \sin \frac{\pi(k+1)(n+1)}{N+1} \quad (2)$$

Where  $0 \leq k, n \leq N-1$

### 2.3 Real Fourier

The Real Fourier of a finite real data sequence  $\{f(m)\}$  of length N(even) is defined as[17]

$$\left. \begin{aligned} F(k) &= \frac{1}{N} \sum_{m=0}^{N-1} \sin \frac{\pi(k+1)(2m+1)}{2N} \\ F(k+1) &= \frac{1}{N} \sum_{m=0}^{N-1} \cos \frac{\pi(k+1)(2m+1)}{2N}, k = 0, 2, \dots, (N-2) \end{aligned} \right\} \quad (3)$$

Where

$$f(m) = 2 \sum_{\substack{k=0 \\ k=even}}^{N-2} F(k) \sin \frac{\pi(k+1)(2m+1)}{2N} +$$

$$2 \sum_{\substack{k=0 \\ k=even}}^{N-2} F(k+1) \cos \frac{\pi(k+1)(2m+1)}{2N}, m = 0, 1, \dots, (N-1) \quad (4)$$

### 2.4 Discrete Hartley Transform

The Discrete Hartley Transform (DHT) pair is defined for a real-valued length-N sequence  $x(n)$ ,  $0 \leq n \leq N-1$ , by the following equation

$$H(k) = \sum_{n=0}^{N-1} x(n) \text{cas} \left( \frac{2\pi}{N} kn \right) \quad 0 \leq k \leq N-1 \quad (5)$$

$$x(n) = \frac{1}{N} \sum_{k=0}^{N-1} H(k) \text{cas} \left( \frac{2\pi}{N} kn \right) \quad 0 \leq n \leq N - 1 \quad (6)$$

Where  $\text{cas}(x) = \cos(x) + \sin(x)$

The symmetry of the transform pair is a valuable feature of the DHT.

### 2.5 Discrete Fourier Transform

A discrete formulation of the Fourier transform, which takes place at regularly spaced data values, and returns the value of the Fourier transform for a set of values in frequency space which are equally spaced. The 2D DFT is given as

$$F(u, v) = \frac{1}{NM} \sum_{x=0}^{N-1} \sum_{y=0}^{M-1} f(x, y) e^{-2\pi i \left( \frac{xu}{N} + \frac{yv}{M} \right)} \quad (7)$$

## 3. KEY BASED IMAGE SCRAMBLING IN TRANSFORM DOMAIN

In this paper we are presenting a novel approach for Image scrambling involving both the spatial as well as transform domain. As we know whenever a transform is applied to an image, image is converted from spatial domain to transform domain, and transform coefficients are obtained. To obtain the original image the inverse transform is applied to the transform coefficients. But if the transform coefficients are affected due to any transformation we will not obtain the original image. Using this concept in this paper we have used Key based scrambling[18] which is based on the Random numbers generation based on the size of the image is used for scrambling purpose. The proposed approach is not limited to a particular scrambling method or a transform, the said approach can make use of any scrambling technique or transform on the image.

### 3.1 Image Scrambling

Following are the steps used for Image Scrambling

- 1) Read the image, convert it to grayscale
- 2) Apply a Transform on the image
- 3) Transform coefficients which are obtained in step 2 are now scrambled using key based scrambling method.
- 4) Apply inverse transform on the scrambled transform coefficients obtained in step 3.
- 5) The image obtained in spatial domain will now be scrambled

The scrambling process is also shown in the figure 1.

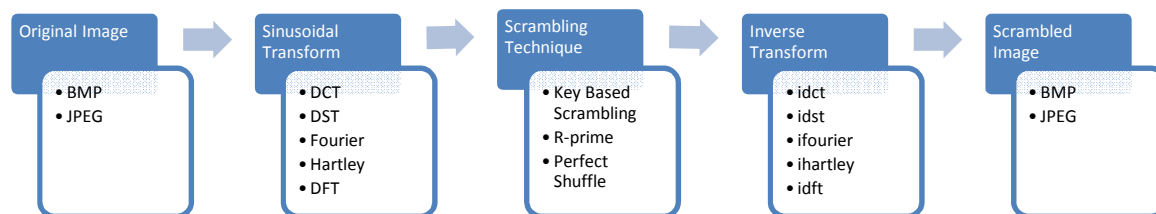


**FIGURE 1:** This Different Steps of Scrambling Process.

### 3.2 Image Descrambling

The descrambling process is as follows

- 1) Read the scrambled image
- 2) Apply the Transform on the image
- 3) Transform coefficients which are obtained in step 2 are now descrambled using key based descrambling method.
- 4) Apply inverse transform on the descrambled transform coefficients obtained in step 3.
- 5) The image obtained in spatial domain will now be original Image

The descrambling process is also shown in the figure 2.

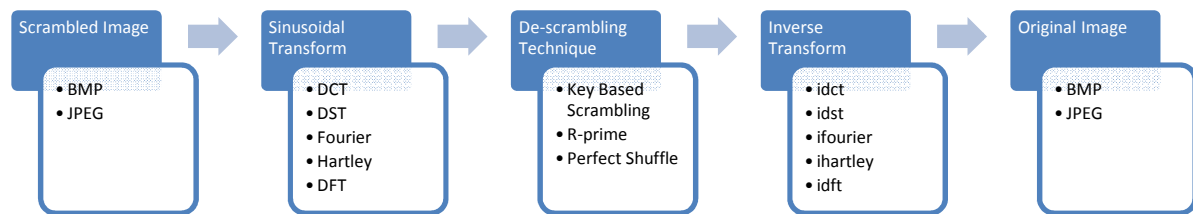


**FIGURE 2:** This Different Steps of De-Scrambling Process.

## 4. EXPERIMENTAL RESULTS

For Experimental purpose, five images of size 256X256 were used with all the five sinusoidal transforms. Figure 3(a) shows the Original Image which is a 24-bit color image which is first converted to grayscale as shown in Figure 3(b), Although the novel approach proposed can also be extended on 24-bit color images.

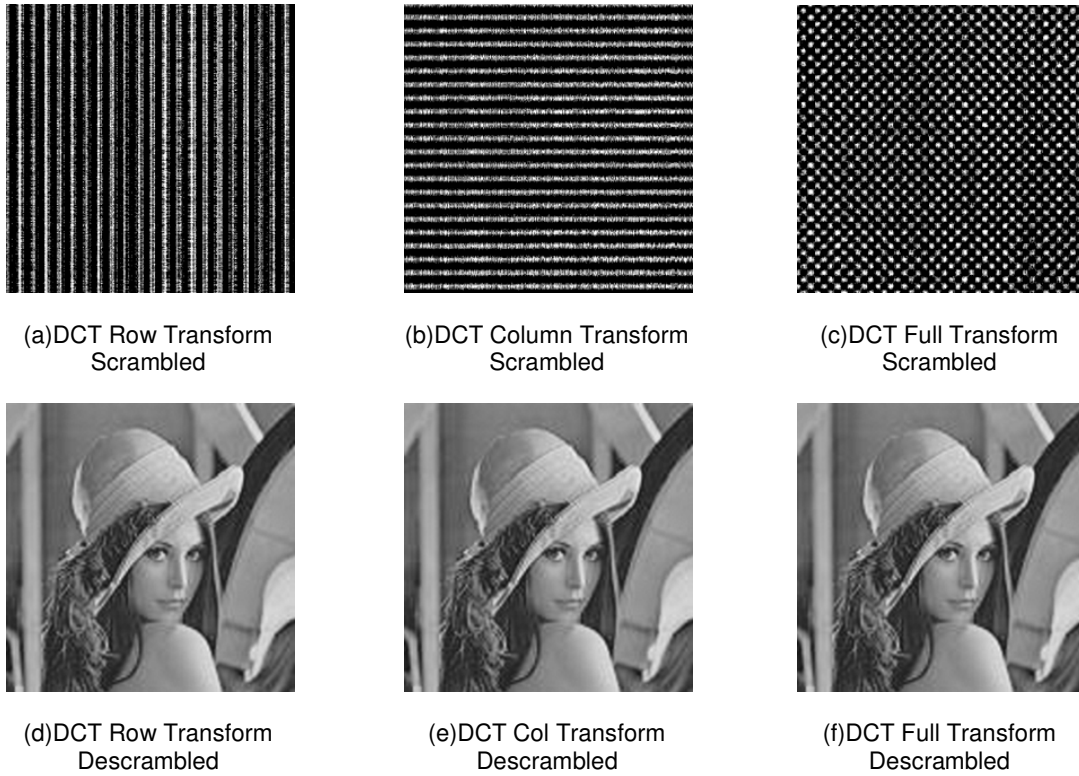


(a) Original Image

(b) Gray Image

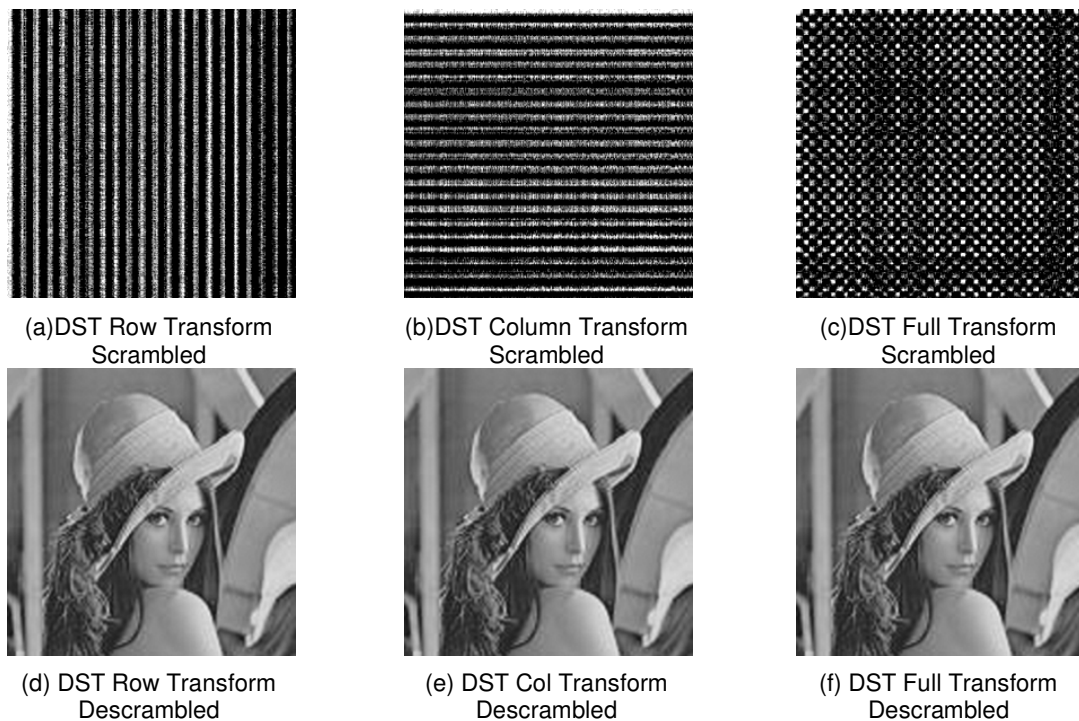
**FIGURE 3**

Figure 4(a-c) shows the scrambled images obtained in spatial domain by applying DCT row, DCT Column and DCT Full transform along with Key-based scrambling on the grayscale images. The descrambled images obtained after applying the descrambling steps are shown in Figure 4(d-f).



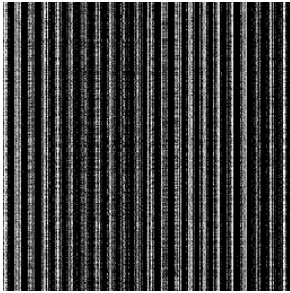
**FIGURE 4**

Figure 5(a-c) shows the scrambled images obtained in spatial domain by applying DST row, DST Column and DST Full transform along with Key-based scrambling on the grayscale images. The descrambled images obtained after applying the descrambling steps are shown in Figure 5(d-f).



**FIGURE 5**

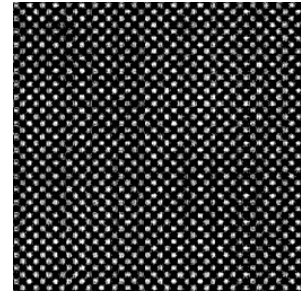
Figure 6(a-c) shows the scrambled images obtained in spatial domain by applying Real Fourier row, Real Fourier Column and Real Fourier Full transform along with Key-based scrambling on the grayscale images. The descrambled images obtained after applying the descrambling steps are shown in Figure 6(d-f).



(a)Real Fourier Row Transform Scrambled



(b)Real Fourier Column Transform Scrambled



(c)Real Fourier Full Transform Scrambled



(d)Real Fourier Row Transform descrambled



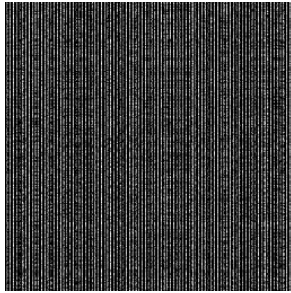
(e)Real Fourier Column Transform descrambled



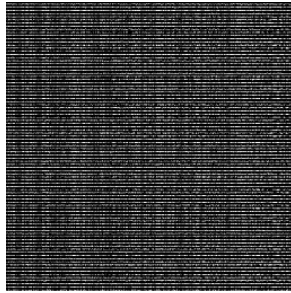
(f)Real Fourier Full Transform descrambled

**FIGURE 6**

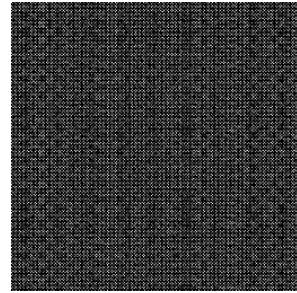
Figure 7(a-c) shows the scrambled images obtained in spatial domain by applying Hartley row, Hartley Column and Hartley Full transform along with Key-based scrambling on the grayscale images. The descrambled images obtained after applying the descrambling steps are shown in Figure 7(d-f).



(a)Hartley Row Transform Scrambled



(b)Hartley Column Transform Scrambled



(c)Hartley Full Transform Scrambled



(d)Hartley Row Transform descrambled



(e)Hartley Column Transform descrambled



(f)Hartley Full Transform descrambled

**FIGURE 7**

Figure 8(a-c) shows the scrambled images obtained in spatial domain by applying DFT row, DFT Column and DFT Full transform along with Key-based scrambling on the grayscale images. The descrambled images obtained after applying the descrambling steps are shown in Figure 8(d-f).

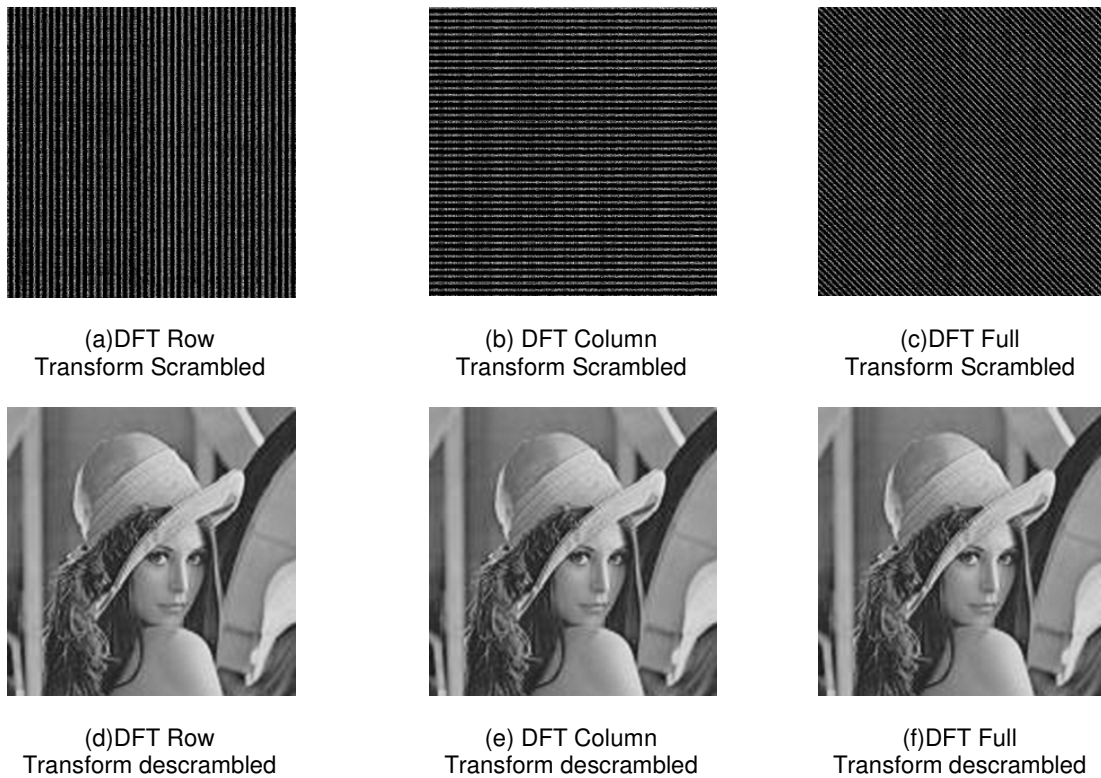


FIGURE 8

Original Image :Lena [ Row: 0.8439 and col: 0.6937]						
Transform	Row Transform	Row Transform Scrambled	Column Transform	Column Transform Scrambled	Full Transform	Full Transform Scrambled
DCT	Row: 0.9938 Col: 0.1958	Row: 0.5546 Col: 0.3890	Row: 0.1907 Col: 0.9932	Row: 0.4802 Col: 0.6521	Row: 0.2062 Col: 0.2202	Row: 0.5576 Col: 0.5835
DST	Row: 0.9940 Col: 0.2079	Row: 0.5383 Col: 0.3316	Row: 0.1910 Col: 0.9909	Row: 0.4543 Col: 0.5676	Row: 0.3048 Col: 0.3395	Row: 0.5271 Col: 0.5232
Real Fourier	Row: 0.9956 Col: 0.2131	Row: 0.5771 Col: 0.2237	Row: 0.1901 Col: 0.9930	Row: 0.4507 Col: 0.2054	Row: 0.2093 Col: 0.2345	Row: 0.3222 Col: 0.2601
Hartley	Row: 0.9947 Col: 0.2136	Row: 0.2385 Col: 0.2224	Row: 0.2160 Col: 0.9931	Row: 0.1969 Col: 0.2175	Row: 0.3966 Col: 0.4995	Row: 0.2096 Col: 0.2048
DFT	Row: 0.9961 Col: 0.1736	Row: 0.2697 Col: 0.1677	Row: 0.1860 Col: 0.9961	Row: 0.1308 Col: 0.2117	Row: 0.4178 Col: 0.4599	Row: 0.1877 Col: 0.1780

Original Image :Pepper [ Row: 0.8891 and col: 0.8468]						
Transform	Row Transform	Row Transform Scrambled	Column Transform	Column Transform Scrambled	Full Transform	Full Transform Scrambled
DCT	Row: 0.9926 Col: 0.1890	Row: 0.5381 Col: 0.3483	Row: 0.1888 Col: 0.9932	Row: 0.4156 Col: 0.6019	Row: 0.2278 Col: 0.3145	Row: 0.5571 Col: 0.5680
DST	Row: 0.9919 Col: 0.1892	Row: 0.5707 Col: 0.3907	Row: 0.2013 Col: 0.9899	Row: 0.3830 Col: 0.5207	Row: 0.3547 Col: 0.2044	Row: 0.4879 Col: 0.5080
Real Fourier	Row: 0.9955 Col: 0.2018	Row: 0.5126 Col: 0.2291	Row: 0.1892 Col: 0.9929	Row: 0.3722 Col: 0.2334	Row: 0.2384 Col: 0.2374	Row: 0.4108 Col: 0.3003
Hartley	Row: 0.9941 Col: 0.2004	Row: 0.3166 Col: 0.1965	Row: 0.2032 Col: 0.9933	Row: 0.1857 Col: 0.2439	Row: 0.5053 Col: 0.5722	Row: 0.2656 Col: 0.2227
DFT	Row: 0.9961 Col: 0.1559	Row: 0.3901 Col: 0.1383	Row: 0.1605 Col: 0.9961	Row: 0.1265 Col: 0.2696	Row: 0.4932 Col: 0.5445	Row: 0.2429 Col: 0.2116

Original Image :Lotus [ Row: 0.8163 and col: 0.8461]						
Transform	Row Transform	Row Transform Scrambled	Column Transform	Column Transform Scrambled	Full Transform	Full Transform Scrambled
DCT	Row:0.9839 Col: 0.1847	Row: 0.3744 Col: 0.4335	Row: 0.1950 Col: 0.9915	Row: 0.3806 Col: 0.4547	Row: 0.2391 Col: 0.2292	Row: 0.4567 Col: 0.5137
DST	Row: 0.9795 Col: 0.1901	Row: 0.4459 Col: 0.4601	Row: 0.1996 Col: 0.9879	Row: 0.3821 Col: 0.2824	Row:0.3615 Col: 0.3170	Row: 0.4182 Col: 0.4148
Real Fourier	Row: 0.9918 Col: 0.1914	Row: 0.3810 Col: 0.2458	Row: 0.2012 Col: 0.9892	Row: 0.3649 Col: 0.2126	Row: 0.2531 Col: 0.2311	Row: 0.2906 Col: 0.3091
Hartley	Row: 0.9884 Col: 0.2290	Row: 0.2134 Col: 0.2146	Row: 0.1860 Col: 0.9915	Row: 0.2061 Col: 0.2148	Row: 0.3902 Col: 0.4168	Row: 0.2153 Col: 0.1902
DFT	Row: 0.9939 Col: 0.1908	Row: 0.2007 Col: 0.1426	Row: 0.1369 Col: 0.9954	Row: 0.1415 Col: 0.2143	Row: 0.3442 Col: 0.3701	Row: 0.1844 Col: 0.1405

Original Image :Baboon [ Row: 0.7179 and col: 0.6935]						
Transform	Row Transform	Row Transform Scrambled	Column Transform	Column Transform Scrambled	Full Transform	Full Transform Scrambled
DCT	Row: 0.9912 Col: 0.2006	Row: 0.6365 Col: 0.3851	Row: 0.2721 Col: 0.9935	Row: 0.3866 Col: 0.6583	Row: 0.2778 Col: 0.2159	Row:0.5723 Col: 0.5739
DST	Row: 0.9923 Col: 0.2029	Row: 0.7196 Col: 0.3702	Row: 0.2912 Col: 0.9927	Row: 0.3789 Col: 0.5446	Row: 0.3865 Col: 0.3444	Row:0.4690 Col: 0.5042
Real Fourier	Row: 0.9953 Col: 0.2096	Row: 0.6600 Col: 0.2457	Row: 0.1987 Col: 0.9937	Row: 0.3794 Col: 0.1922	Row: 0.2179 Col: 0.2179	Row:0.2420 Col: 0.2749
Hartley	Row: 0.9928 Col: 0.2144	Row: 0.2002 Col: 0.2370	Row: 0.2633 Col: 0.9937	Row: 0.1911 Col: 0.1918	Row: 0.4242 Col: 0.3475	Row:0.1825 Col: 0.1937
DFT	Row: 0.9961 Col: 0.1684	Row: 0.1945 Col: 0.1575	Row: 0.2569 Col: 0.9961	Row: 0.1350 Col: 0.1754	Row: 0.3952 Col: 0.2750	Row:0.1422 Col: 0.1430

Original Image :Cartoon [ Row: 0.8027 and col: 0.8070]						
Transform	Row Transform	Row Transform Scrambled	Column Transform	Column Transform Scrambled	Full Transform	Full Transform Scrambled
DCT	Row: 0.9945 Col: 0.1887	Row: 0.7014 Col: 0.5178	Row: 0.2556 Col: 0.9955	Row: 0.5230 Col: 0.7489	Row: 0.2897 Col: 0.2238	Row:0.6601 Col: 0.6596
DST	Row: 0.9944 Col:0.2056	Row: 0.8154 Col: 0.4576	Row: 0.2646 Col: 0.9953	Row: 0.4515 Col: 0.6254	Row: 0.3048 Col: 0.5047	Row: 0.5924 Col: 0.5571
Real Fourier	Row: 0.9959 Col: 0.2185	Row: 0.7298 Col: 0.2971	Row: 0.2217 Col: 0.9954	Row: 0.4903 Col: 0.2254	Row: 0.2613 Col: 0.2383	Row: 0.3178 Col: 0.3187
Hartley	Row: 0.9949 Col: 0.2605	Row: 0.2700 Col: 0.2675	Row: 0.1983 Col:0.9954	Row: 0.2046 Col: 0.2337	Row: 0.3954 Col: 0.5162	Row:0.2412 Col: 0.2146
DFT	Row: 0.9961 Col: 0.2406	Row: 0.3027 Col: 0.1623	Row: 0.1492 Col: 0.9961	Row: 0.1299 Col: 0.2483	Row: 0.3068 Col: 0.4806	Row: 0.2410 Col: 0.1872

**TABLE 1:** Average Row and Average Column correlation obtained in Row Transform , Row Transform scrambled , Column Transform , Column Transform Scrambled , Full Transform and Full Transform scrambled images for DCT, DST, Real Fourier , Hartley and DFT Transforms

The Figure 9 – Figure 13 shows the blockwise cumulative energy in the transform coefficients after applying row transform, column transform and full transform. Energy in the coefficients is calculated by dividing the image in to blocks. The first block is of size 2x2 ,the second block considered is 4X4 which includes the first block and an increase in the block size by 2 and so on.

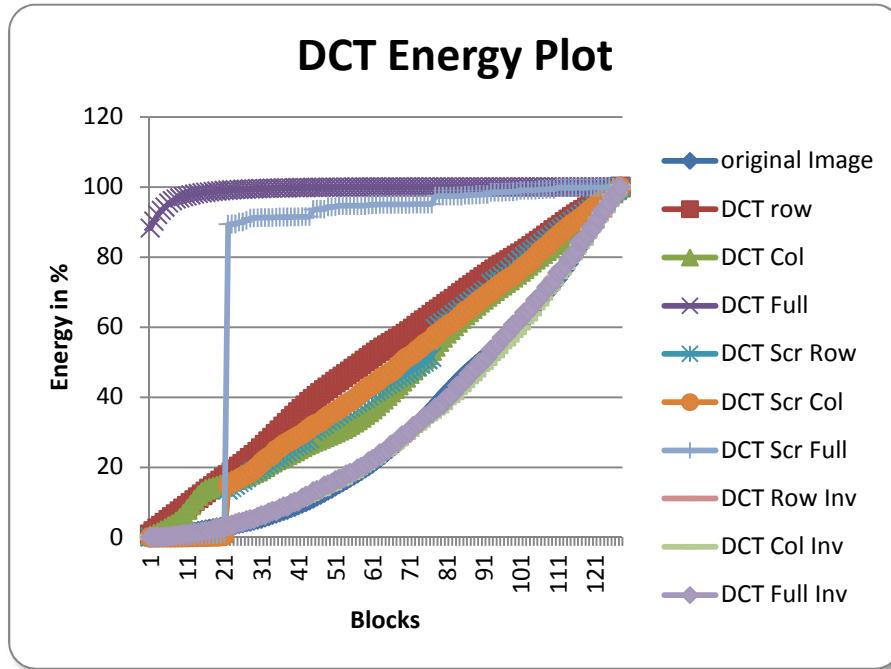


**FIGURE 9:** Block wise Energy obtained in original, DCT row, DCT column, DCT full, DCT row scrambled, DCT Column Scrambled, DCT Full scrambled, DCT row Inverse scrambled, DCT col Inverse scrambled, and DCT full Inverse scrambled.

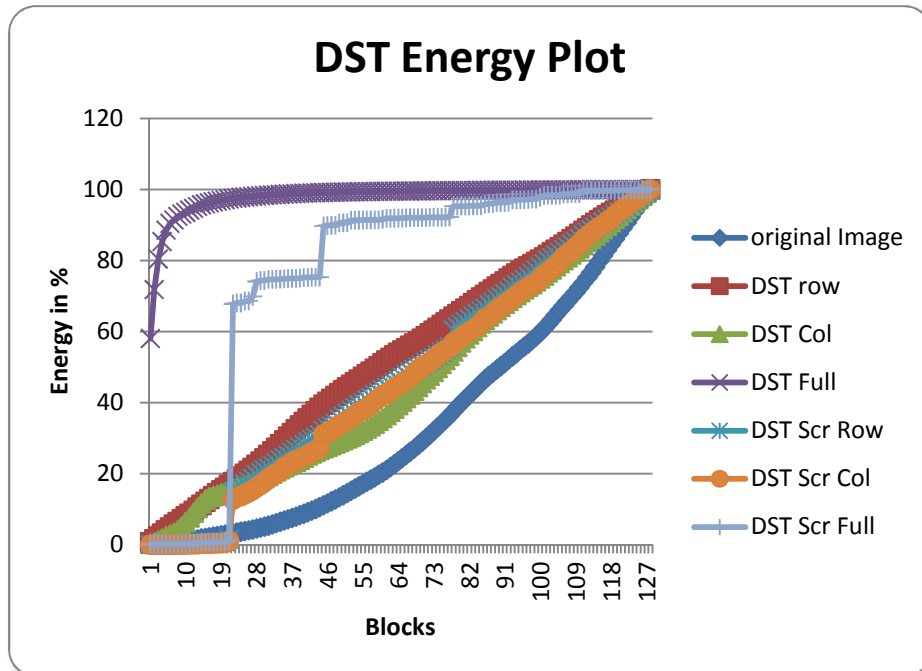


**FIGURE 10:** Block wise Energy obtained in original, DST row, DST column, DST full, DST row scrambled, DST Column Scrambled, and DST Full scrambled.

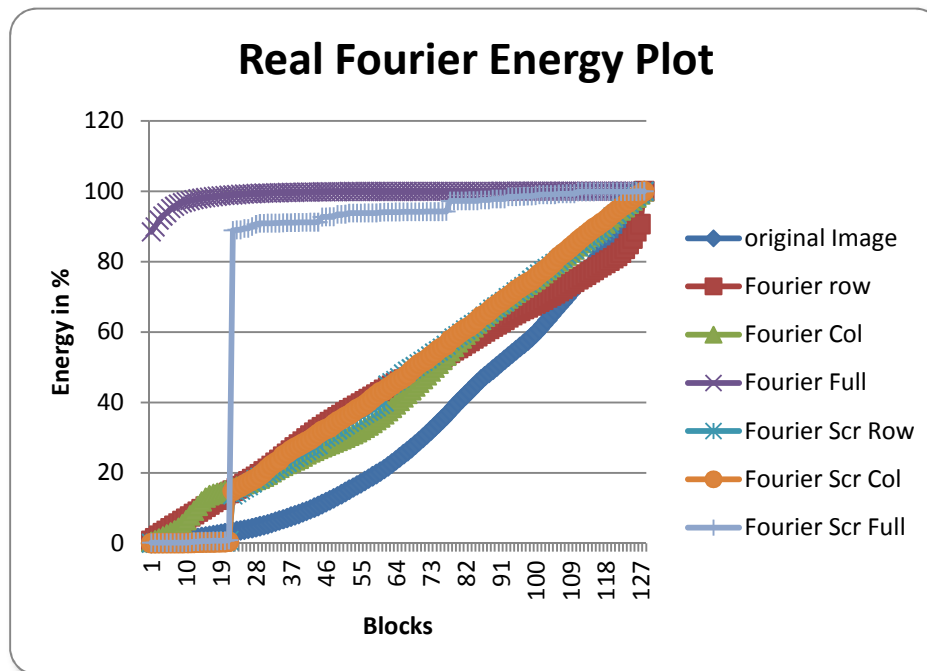


**FIGURE 11:** Block wise Energy obtained in original, Real Fourier row, Real Fourier column, Real Fourier full, Real Fourier row scrambled, Real Fourier Column Scrambled, and Real Fourier Full scrambled.

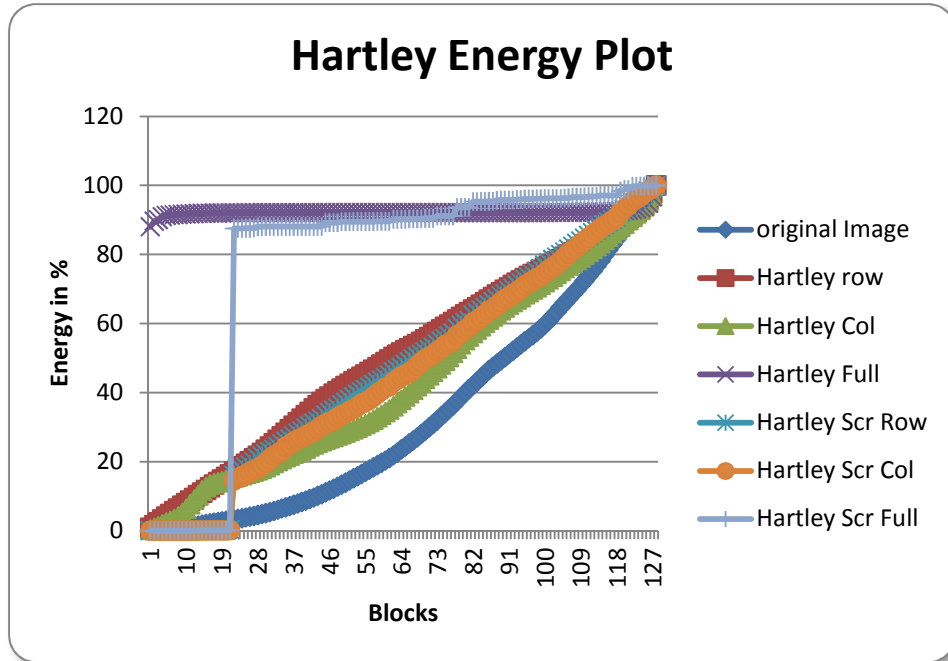


**FIGURE 12:** Block wise Energy obtained in original, Hartley row, Hartley column, Hartley full, Hartley row scrambled, Hartley Column Scrambled, and Hartley Full scrambled.

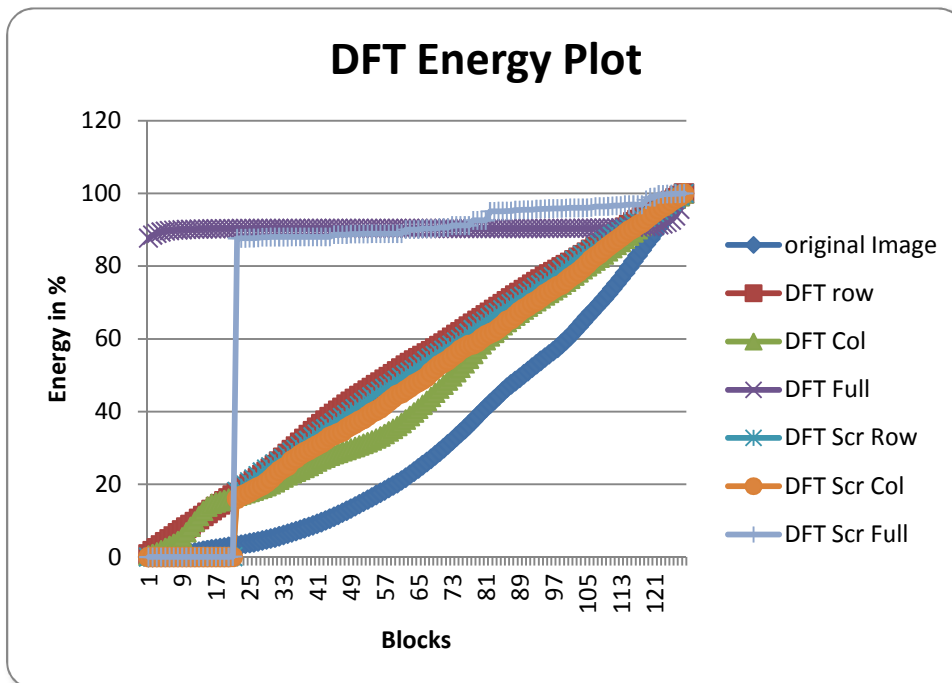


**FIGURE 13:** Block wise Energy obtained in original, DFT row, DFT column, DFT full, DFT row scrambled, DFT Column Scrambled, and DFT Full scrambled.

## 5. EXPERIMENTAL RESULTS DISCUSSION

A Transform is a technique for converting a signal into elementary frequency components. Transform coding relies on the premise that pixels in an image exhibit a certain level of correlation with their neighboring pixels. consequently, these correlations can be exploited using Image Scrambling techniques. The main goal of an Image Scrambling is to decorrelate the image pixels as much as possible so that image data is scrambled and appears in an unreadable format. Reducing the correlation between the rows and columns of the image will be helpful for any scrambling technique. Using this as an experimental parameter, Average correlation between rows and columns is calculated. As we know that applying a transform on the image decorrelates the image pixels, to find out whether a further reduction of this correlation can be obtained by our novel approach, five sinusoidal transforms were tested on a number of images. The experimental results obtained are shown in Table No 1 for five images. The highlighted cells in the Table No 1 show that DHT and DFT proves to be the best in all the three cases of transform applied on a digital image, that is row transform, column transform and full transform. Although the other three that is DCT, DST and Real Fourier gave good results of decorrelation in row transform. However other cases of these three transform does not increase the correlation by a very large value, it is in a marginal range.

To Test these transforms further, we have taken into consideration the energy distribution in original, Transformed and Transform scrambled images. The observations made from the Energy Plot for DCT, DST, Real Fourier, Discrete Hartley and DFT are as follows

Original Image	Row Transformed Image	Column Transformed Image	Full Transformed Image	Row Transform Scrambled Image	Column Transform Scrambled Image	Full Transform Scrambled Image
Linear Increase in energy	Small step linear increase in energy	Small step linear increase in energy	High in the initial blocks and den small increases to reach 100%	Small step linear increase in energy	Small step linear increase in energy	Very less value in the initial blocks and a sudden jump after blocks size >20

## 6. CONCLUSION

In this paper we have presented a Novel Approach for Image scrambling in Transform Domain using Sinusoidal Transforms like DCT, DST, Real Fourier, Hartley and DFT. From the experimental results it is clear that our proposed approach can be used for secured image scrambling. The Correlation obtained for Discrete Hartley and DFT proves to be very less which was our main goal of Image scrambling. The energy plot observations can also be used as a measure for detecting Image scrambling in transform domain for full sinusoidal transforms. The Proposed Approach is a combination of both transform as well as spatial domain, hence it is very useful for Image scrambling and provides more security.

In the previous case[19], we have found that Kekre transform gave the best performance as compared to all other Non Sinusoidal transforms. The transforms used in this paper gave the performance close to Kekre transform with DFT and Discrete Hartley proving better than that.

## 7. REFERENCES

- [1] J.-L. Fan and X.-F. Zhang, "Image encryption algorithm based on chaotic system," in *International Conference on Computer-Aided Industrial Design and Conceptual Design. CAIDCD, 2006*, pp. 1–6.
- [2] Chen, C.L.P, Tong Zhang , Yicong Zhou, "Image encryption algorithm based on a new combined chaotic system", *IEEE International Conference on Systems, Man, and Cybernetics (SMC), 2012*, pp. 2500 – 2504
- [3] M. Jian-liang, P. Hui-jing, and G. Wan-qing, "New color image encryption algorithm based on chaotic sequences ranking," in *Proceedings of the International Conference on Intelligent Information Hiding and Multimedia Signal Processing, 2008. IIHMS'08*, August 2008, pp. 1348–1351.
- [4] Lei Li-hong; Bai Feng-ming; Han Xue-hui, "New Image Encryption Algorithm Based on Logistic Map and Hyper-Chaos," *Fifth International Conference on Computational and Information Sciences (ICIS), 2013*, vol., no., pp.713,716, 21-23 June 2013
- [5] Naeem, E.A.; Elnaby, M.M.A.; Hadhoud, M.M., "Chaotic image encryption in transform domains," *International Conference on Computer Engineering & Systems, 2009. ICCES 2009.*, vol., no., pp.71-76, 14-16 Dec. 2009.
- [6] Sapna Anoop, Anoop Alakkaran, "A Full Image Encryption Scheme Based on Transform Domains and Stream Ciphers", *International Journal of Advanced Information Science and Technology (IJAIST)*, Vol. 17, pp. 5-10, September 2013
- [7] Long Bao , Yicong Zhou , C. L. Philip Chen, "Image encryption in the wavelet domain", in *Proc. SPIE 8755, Mobile Multimedia/Image Processing, Security, and Applications 2013*
- [8] Taranjit Kaur, Reecha Sharma, "Image Cryptography by TJ-SCA: Supplementary Cryptographic Algorithm for Color Images", *International Journal of Scientific & Engineering Research*, Volume 4, Issue 7, pp 1355-1360, July-2013.
- [9] Y. Zhou, K. Panetta, S. Agaian, and C. L. P. Chen, "Image encryption using P- Fibonacci transform and decomposition," *Optics Communications*, vol. 285, pp. 594-608, 2012.
- [10] K. Wong and K Tanaka, "Scalable Image Scrambling Method Using Unified Constructive Permutation Function on Diagonal Blocks," *IEEE Proc. 28<sup>th</sup> Picture Coding Symposium PCS*, pp. 138-141, 2010.
- [11] Liu, S., Sheridan, J.T.: Optical Information Hiding by Combining Image Scrambling Techniques in Fractional Fourier Domains. In: Irish Signal and Systems Conference, pp. 249–254, 2001.
- [12] C. Li, G. Xu, C. Song and J. Jing, "Evaluation of Image Scrambling Degree with Intersecting Cortical Model Neural Network", *International Journal of Hybrid Information Technology*, Vol. 5, No. 2, pp. 31-40, 2012.
- [13] M François, T Grosgees, D Barchiesi, R Erra, "Image Encryption Algorithm Based on a Chaotic Iterative Process", *Applied Mathematics*, Vol. 3, No. 12, 2012, pp. 1910-1920.
- [14] Mishra, Minati, Priyadarsini Mishra, M. C. Adhikary, and Sunit Kumar. "Image Encryption Using Fibonacci-Lucas Transformation." *International Journal on Cryptography and Information Security (IJCIS)*, Vol.2, No.3, September 2012 pp 131-141

- [15]Zhu, Guiliang, Weiping Wang, Xiaoqiang Zhang, and Mengmeng Wang. "Digital image encryption algorithm based on pixels." In Intelligent Computing and Intelligent Systems (ICIS), 2010 IEEE International Conference on, vol. 1, pp. 769-772. IEEE, 2010.
- [16]Feng, Yong, and Xinghuo Yu. "A novel symmetric image encryption approach based on an invertible two-dimensional map." In Industrial Electronics, 2009. IECON'09. 35th Annual Conference of IEEE, pp. 1973-1978. IEEE, 2009.
- [17]H.B.Kekre and J.K.Solanki, "Comparative performance of various trigonometric unitary transforms for transform image coding" , International Journal of Electronics, Vol. 44, No. 3. pp. 305-315, 1978.
- [18]P. Premaratne & M. Premaratne, "Key-based scrambling for secure image communication," in Emerging Intelligent Computing Technology and Applications, P. Gupta, D. Huang, P. Premaratne & X. Zhang, Ed. Berlin: Springer, 2012, pp.259-263.
- [19] H.B.Kekre, Tanuja Sarode, Pallavi Halarnkar, Debkanya Mazumder, "Image Scrambling using Non Sinusoidal transforms and Key based Scrambling Technique", International Journal of Computer Technology (IJCT), Volume 12 issue no 8, pp. 3809- 3822. February 2014.

## INSTRUCTIONS TO CONTRIBUTORS

The *International Journal of Image Processing (IJIP)* aims to be an effective forum for interchange of high quality theoretical and applied research in the Image Processing domain from basic research to application development. It emphasizes on efficient and effective image technologies, and provides a central forum for a deeper understanding in the discipline by encouraging the quantitative comparison and performance evaluation of the emerging components of image processing.

We welcome scientists, researchers, engineers and vendors from different disciplines to exchange ideas, identify problems, investigate relevant issues, share common interests, explore new approaches, and initiate possible collaborative research and system development.

To build its International reputation, we are disseminating the publication information through Google Books, Google Scholar, Directory of Open Access Journals (DOAJ), Open J Gate, ScientificCommons, Docstoc and many more. Our International Editors are working on establishing ISI listing and a good impact factor for IJIP.

The initial efforts helped to shape the editorial policy and to sharpen the focus of the journal. Starting with Volume 9, 2015, IJIP will be appearing with more focused issues. Besides normal publications, IJIP intends to organize special issues on more focused topics. Each special issue will have a designated editor (editors) – either member of the editorial board or another recognized specialist in the respective field.

We are open to contributions, proposals for any topic as well as for editors and reviewers. We understand that it is through the effort of volunteers that CSC Journals continues to grow and flourish.

### LIST OF TOPICS

The realm of International Journal of Image Processing (IJIP) extends, but not limited, to the following:

- Architecture of imaging and vision systems
- Character and handwritten text recognition
- Chemistry of photosensitive materials
- Coding and transmission
- Color imaging
- Data fusion from multiple sensor inputs
- Document image understanding
- Holography
- Image capturing, databases
- Image processing applications
- Image representation, sensing
- Implementation and architectures
- Materials for electro-photography
- New visual services over ATM/packet network
- Object modeling and knowledge acquisition
- Photographic emulsions
- Autonomous vehicles
- Chemical and spectral sensitization
- Coating technologies
- Cognitive aspects of image understanding
- Communication of visual data
- Display and printing
- Generation and display
- Image analysis and interpretation
- Image generation, manipulation, permanence
- Image processing: coding analysis and recognition
- Imaging systems and image scanning
- Latent image
- Network architecture for real-time video transport
- Non-impact printing technologies
- Photoconductors
- Photopolymers

- Prepress and printing technologies
- Remote image sensing
- Storage and transmission

- Protocols for packet video
- Retrieval and multimedia
- Video coding algorithms and technologies for ATM/p

## **CALL FOR PAPERS**

---

**Volume: 9 - Issue: 2**

**i. Submission Deadline :** January 31, 2015      **ii. Author Notification:** February 28, 2015

**iii. Issue Publication:** March/April 2015

## **CONTACT INFORMATION**

### **Computer Science Journals Sdn Bhd**

B-5-8 Plaza Mont Kiara, Mont Kiara

50480, Kuala Lumpur, MALAYSIA

Phone: 006 03 6204 5627

Fax: 006 03 6204 5628

Email: [cscpress@cscjournals.org](mailto:cscpress@cscjournals.org)

CSC PUBLISHERS © 2014  
COMPUTER SCIENCE JOURNALS SDN BHD  
B-5-8 PLAZA MONT KIARA  
MONT KIARA  
50480, KUALA LUMPUR  
MALAYSIA

PHONE: 006 03 6204 5627

FAX: 006 03 6204 5628

EMAIL: [cscpress@cscjournals.org](mailto:cscpress@cscjournals.org)